UNIVERSITÀ DEGLI STUDI DI PADOVA

Dipartimento di Fisica e Astronomia "Galileo Galilei"

Master Degree in Physics

Final Dissertation

Classical simulation of noisy quantum gates on different quantum hardware platforms

Thesis supervisor

Dr. Ilaria Siloi

Thesis co-supervisor

Prof. Simone Montangero

Candidate

David-Gabriel Lange

Academic Year 2023/24

Abstract

The open dynamics of single- and multi-qubit systems are governed by the Lindblad equation. Thus, by solving the underlying Hamiltonian including the relevant Lindblad operators for specific gates, an algorithm can be revised that simulates quantum operations incorporating Markovian noise. By integrating suitable stochastic and deterministic noise terms into the logical gate, a novel noisy gate can be manufactured replacing the exact gate. In this work, we implement such a solution for single- and two-qubit operations on both the superconducting as well as the Rydberg architecture. With the prospect of comparing the resemblance with a real quantum computer, we show that the behaviour of our implementation is consistent with the exact solution of the underlying Lindblad equation.

Contents

Listing of figures

Listing of acronyms

NISQ ..... Noisy Intermediate-Scale Quantum

SDE ..... Stochastic Schrödinger equation

QHO ..... Quantum harmonic oscillator

SC ..... Superconducting

CPB ..... Cooper pair box

CR ..... Cross resonance

RWA ..... Rotating wave approximation

Introduction

The concept of a quantum computer, initially conceived by Richard Feynman in the 1980s, entails using quantum systems to simulate the fundamental constituents of matter. This idea has spurred the development of quantum simulators - controllable quantum systems tailored for specific applications, such as exploring complex phases or out-of-equilibrium phenomena in condensed matter systems. On the other hand, Feynman's idea has rapidly established the field of quantum computation, and with it the development of quantum algorithms, that leverage on the properties of quantum mechanics, including superposition and entanglement, to speed up specific computational processes [1]. These general-purpose quantum computers aim for broader computational capabilities, and current efforts are focused on achieving quantum supremacy, demonstrating a quantum computer's ability to solve problems beyond classical counterparts.

A great challenge lies in constructing universal fault-tolerant quantum computers [2]. Despite the development of quantum error-correcting algorithms, their practical implementation is constrained by the quantity and quality of qubits, the quantum counterparts to classical bits, available in current hardware [3]. Our quantum computing era is thus called Noisy-Intermediate-Scale-Quantum (NISQ) era, wherein all quantum platforms are subjected to noise, arising from diverse sources, and responsible for the degradation of the quantum properties. In the current era, we cope with the introduced errors in the machines, and it is imperative to establish efficient ways to mitigate and correct them. To this aim it is paramount to identify, characterize and simulate the noise in quantum computers to have optimized calibration protocols and error correcting codes, which are necessary for large-scale quantum computation.

Nowadays, the most established quantum computing platforms include superconducting circuits, trapped ions and neutral atoms, such as Rydberg atoms. On each platform, an effective two-level system is obtained to represent a single qubit, while gate operations are implemented as sequences of pulses acting on the qubit(s). In all these architectures, noise is a major limiting factor and therefore, our effort is

aimed at understanding and modeling the noise at the gate level. In this work, we will address this question for two systems, the superconducting and the Rydberg hardware. Superconducting qubits are derived from resonant LC circuits where the inductor is replaced by a Josephson junction to introduce anharmonicity into the energy spectrum. Rydberg atoms, on the other hand, are special type of atoms, where one or more valence electrons are excited to high lying states, so called Rydberg states. The quantum information is stored in two atomic levels, while the Rydberg level is used to drive controlled interactions. Rydberg based architectures are especially promising nowadays, because of their large scalability [4]. Furthermore, recently it has been shown that an implementation of a two-qubit controlled-phase gate on a strontium-88 platform can be achieved with a Bell-state fidelity as high as 99.9% [5].

Usually, the simulation of noisy quantum computers is implemented at the density matrix level by adding appropriate quantum operations before and after each ideal gate. This work is based on a recent publication [6], where a novel way of modelling NISQ devices is introduced, by integrating a description of Markovian noise into the used logical gates. This approach allows the description of the physics occurring during the execution of gate. Here, we work at the state vector level by including stochastic operators to account for the noisy dynamics. The basic idea can be sketched as

$$|\psi_0\rangle \; \boxed{\mathcal{G}_\xi} \; |\psi_1\rangle \,, \tag{0.1}$$

where $\mathcal{G}_\xi$ is the solution to a stochastic Schrödinger equation that incorporates both the dynamics that generate the ideal gate and the noise caused by the environment. In this way, one run of the simulation can be seen as the corresponding run on the actual hardware. In order to implement this idea, the general working principle consists of finding the ideal gates of the process, understanding which noises are contributing and then replacing each ideal gate with the corresponding noisy one.

In this Thesis we successfully implemented this novel approach that allows for an improved and more efficient simulation of NISQ computers. We tested the protocol on superconducting qubits and extended the method to Rydberg atoms. Our simulations were compared to the theoretical predictions of the Lindblad equation

for the dynamics, however we plan on accessing the actual hardware as the first next step.
The thesis is structured as following:

1. **Introduction to quantum computing, chapter 1**
   We give a short recap of all relevant concepts that are used throughout the work, such as definition of quantum states, density matrices, entanglement and time-evolution. We also explain the qubit and the relevant concepts in quantum information, such as gates, channels and quantum circuits. Lastly, we provide a description of all important noise models we will use.

2. **Noisy gate derivation, chapter 2**
   We derive the noisy gate $\mathcal{G}_\xi$ starting from the stochastic Schrödinger equation, using a perturbative approach which assumes that the execution time of a single gate is much smaller than the characteristic times of the relevant noises.

3. **Example 1: Superconducting qubit, chapter 3**
   We first introduce the superconducting qubit, starting from a quantum mechanical description of an LC circuit. Then we derive the gates that we use to simulate the hardware: the single-qubit not gate and the two-qubit cross resonance (CR) gate. Lastly, we show the results of the simulation and compare it to the exact solution to the differential equation.

4. **Example 2: Rydberg qubit, chapter 4**
   First, we discuss Rydberg atoms in general, before delving into the specifics on how to achieve single- and two-qubit gates on this architecture. Again, we compare the results of the simulation to the exact solution.

1

Introduction to quantum computing

Quantum computing is a new paradigm of computation that processes information using the rules of quantum mechanics. In the chapter we first review fundamental concepts in quantum mechanics such as definition of density matrices, quantum entanglement and the quantum evolution of closed systems. Building upon these elements, we delineate the constituents of a quantum computation starting from the definition of the fundamental unit of information, the qubit, and the subsequent concepts of quantum registers, gates, channels and quantum circuits.

1.1 State representation and density matrices

Following the first postulate of quantum mechanics [7], a Hilbert space, known as state space, is associated to any isolated physical object. The system is completely described by its state vector, a unit vector in the system's state space.
The simplest quantum mechanical system is a two-level system. Given an orthonormal basis, then an arbitrary state vector of this system can be written as

$$|\psi\rangle = c_0 |0\rangle + c_1 |1\rangle , \tag{1.1}$$

where $|c_i|^2$ can be interpreted as the probability of finding the system in the state $|i\rangle$ and the total probability is conserved, i.e. $|c_1|^2 + |c_2|^2 = 1$.

Equation 1.1 can be recast in spherical coordinates

$$|\psi\rangle = \cos\frac{\theta}{2}|0\rangle + e^{i\phi}\sin\frac{\theta}{2}|1\rangle\,, \tag{1.2}$$

with $0 \leq \theta \leq \pi$ and $0 \leq \phi \leq 2\pi$. In this way a qubit can be visualized as a vector pointing on the surface of a unitary sphere (see figure 1.1) uniquely defined by the two angles. The z-axis is called the longitudinal axis and by convention, the $|0\rangle$ state is on the north pole of the sphere. Furthermore, the $x-y$ plane is called the transverse plane.

In analogy to the bits of the classical computer, a quantum computer stores information on these two-level systems, known as as quantum bits or qubits. In all competing architectures, the qubits have two states $|0\rangle$ and $|1\rangle$ that are encoded on different physical systems, such as two hyperfine levels in trapped ions, charge states in a superconducting circuits or polarizations in photons.

Already, the advantage of qubits becomes clear. We can store more information on one qubit than on the classical counterpart. Moreover, the true power emerges when increasing the number of qubits, since the number of combinations between input states grows exponentially in number of qubits. However, we know from quantum mechanics that measurements collapse the wavefunction, thus destroying any superposition and always giving a classical result. Therefore, so far there is no advantage over saving the same numbers in memory on classical bits. However, unlike the classical realm, the superposition can be exploited to parallelize the computation, while quantum entanglement, see section 1.2 allows for completely new operations.

Equation 1.2 provides the conventional method for representing a qubit on the Bloch sphere, see Figure 1.1, offering a valuable visualization of the dynamics of two-level systems. We now have a representation that can be used to visualize how states of qubits transform under unitary transformations as rotations of vectors on the surface of a sphere. An important combination of these rotations is the Hadamard gate, H. In terms of the Bloch sphere, it corresponds to the transformation that moves the state on the north pole, $|0\rangle$, into the superposition state, which lies on the equator of the sphere.

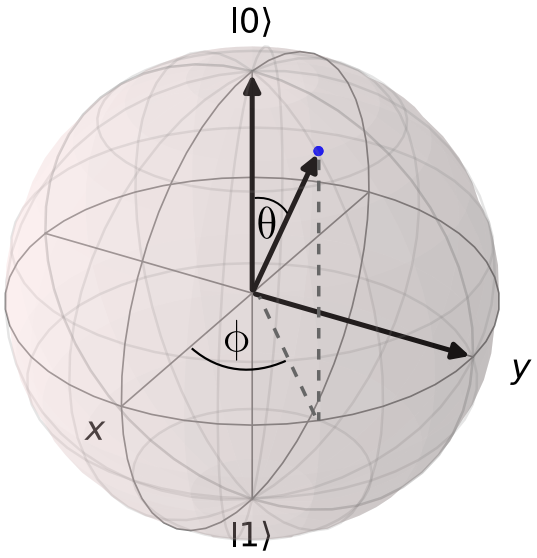

Figure 1.1: Bloch sphere representation of a single qubit state. The angles θ and ϕ define a point on the unit three-dimensional sphere, Bloch sphere, that represents a single qubit. The z-axis corresponds to the Figure was generated using qutip [8].

Unit vectors like 1.1 are called pure states and provide the whole information regarding the system. Otherwise, one can generalize this representation to an ensemble of wave functions ψ_n, each one having a (classical) probability of describing the system, a so-called mixed state. In other words and also experimentally speaking, we more often are working with statistical mixtures of pure states. To characterize pure and mixed states with a unified formalism, we introduce the density matrix [7]. Density matrices are positive semidefinite operators acting on Hilbert spaces. The most general definition of a quantum state via the density matrix is

$$\rho = \sum_{j=1}^{m} p_j \left|\psi_j\right\rangle \left\langle\psi_j\right| = \sum_{i,j=1}^{d} \rho_{ij} \left|\phi_i\right\rangle \left\langle\phi_j\right|, \tag{1.3}$$

where we first introduce a mixture of m states and then express the wave functions in terms of a basis of the Hilbert space $\mathcal{H}$ with dimension d. The diagonal elements are the classical probabilities that the system is in that specific state, while the off-diagonal elements are contributions from coherent superpositions.
Density matrices have the properties,

1. hermitian, i.e. $\rho = \rho^\dagger$;
2. non-negative, i.e. $\langle\psi|\,\rho\,|\psi\rangle \geq 0 \,\forall\, |\psi\rangle \in \mathcal{H}$;
3. $\mathrm{Tr}(\rho) \equiv \sum_{k=1}^{n} \langle k|\,\rho\,|k\rangle = 1$, where $|k\rangle_{k=1\ldots n}$ is a basis of the n-dimensional Hilbert space $\mathcal{H}$ and Tr() is the trace operation;
4. if ρ is pure, then $\rho = |\psi_1\rangle\langle\psi_1|$ since there is only $p_1 = 1$ and every other $p_j = 0 \,\forall\, j \neq 1$ and since ρ is a projector, i.e. $\rho = \rho^\dagger$, $\mathrm{Tr}(\rho^2) = 1$;
5. if ρ is mixed, then $\mathrm{Tr}(\rho^2) < 1$.

The density operator contains all physical information about the system, which can be extracted using the expectation value of some observable A

$$\langle A\rangle = \mathrm{Tr}(A\rho). \tag{1.4}$$

1.2 Composite systems

If we want to simulate more complex systems, such as multiple qubits interacting among each other and the environment, we have to introduce the concept of composite systems [9]. In composite systems, the total state space the many body system resides in is given by the tensor product of each single body Hilbert space

$$\mathcal{H}_N = \mathcal{H}_1 \otimes \mathcal{H}_2 \otimes \ldots \otimes \mathcal{H}_d. \tag{1.5}$$

A more general n-body state can be written as

$$|\psi\rangle = \sum_{i}^{d} c_i\,|\phi_i\rangle\,, \tag{1.6}$$

where again $\{|\phi_i\rangle\}$ form the orthonormal basis set for the considered Hilbert space and any state vector of this system can be attained by choosing different combinations of coefficients under the requirement of normalization, i.e. $\sum_i^d |c_i|^2 = 1$.
If subsequently, we want to focus on a subsystem of this bigger composite system can make use of the reduced density matrix, which can be found by taking the trace over subspaces of the composite Hilbert space, which we are not interested

in

$$\rho_A = \mathrm{Tr}_B(\rho_{AB}) = \sum_n \langle n|_B \, \rho_{AB} \, |n\rangle_B \tag{1.7}$$

and by definition, Eq. 1.7 is a density matrix itself and thus inherits all the properties defined in the previous section.
Here, we can introduce the concept of entanglement, where the power of quantum computation lies. If the wave function of a many-particle system can be written as a product state of each individual component, the quantum state is said to be separable. Moreover, performing an operation on a single state of a composite separable state, like for example a measurement, does not influence the other. If, on the other hand, the composite wave function can not be written as a product state then it is entangled. For example the state

$$\psi = \frac{1}{2}\left[|00\rangle + |01\rangle + |10\rangle + |11\rangle\right] \tag{1.8}$$

does not posses entanglement since it can be expressed as

$$\psi = |A\rangle \, |B\rangle \, , \tag{1.9}$$

with $|A\rangle = 1/\sqrt{2}(|0\rangle + |1\rangle)$ and $|B\rangle = 1/\sqrt{2}(|0\rangle + |1\rangle)$, it is therefore a separable state. While

$$\psi = \frac{1}{\sqrt{2}}\left(|00\rangle + |11\rangle\right) \tag{1.10}$$

is entangled since it can not be decomposed as a simple product of single-particle wavefunctions.
As another example, let us look at the bipartite pure state similar to the qubit, equation 1.2, with $\phi = 0$

$$|\psi\rangle = \cos\frac{\theta}{2}\,|00\rangle + \sin\frac{\theta}{2}\,|11\rangle \, . \tag{1.11}$$

This state is separable if $\theta = 0, \pi$ and entangled otherwise. Moreover, it is maximally entangled when $\theta = \pi/2$, which is referred to as a Bell state. Furthermore, we can quantify the purity of the subsystems by calculating the trace of the re-

duced density matrix squared, i.e. $\mathrm{Tr}(\rho_A^2)$, as seen in figure 1.2. As described before, the state is pure if $\mathrm{Tr}(\rho^2) = 1$ and mixed otherwise. The purity of the reduced density matrix is 1 when the state is separable, while it is < 1 otherwise, since the partial states of a pure and entangled composite state are necessarily mixed.

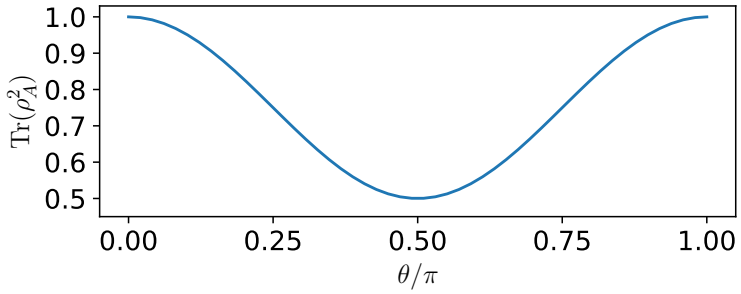

Figure 1.2: Purity of the reduced density matrix for the subsystem A as defined in equation 1.11.

1.3 Evolution of Closed Systems and Quantum Circuits

The closed dynamics of a quantum system are described by the Schrödinger equation

$$H\psi = -\frac{\hbar}{i}\frac{\partial\psi}{\partial t}, \tag{1.12}$$

whose general solution is given by

$$|\psi\rangle = U(t)\,|\psi(0)\rangle = e^{-iHt/\hbar}\,|\psi(0)\rangle\,, \tag{1.13}$$

where $U(t)$ is a unitary operator and is called the time-evolution operator. In the language of quantum computation, when dealing with closed systems, we have a powerful method for manipulating the qubit evolution, namely, through the use of quantum gates. These gates are algebraic objects consisting of unitary operations that act on the quantum states. They allow us to manipulate quantum information without delving into the specifics of the underlying microscopic Hamiltonians that

govern the system's dynamics. Later, we will derive various Hamiltonians for quantum computers that implement these gates and thereby introduce important concepts such as Rabi oscillations.
For now, if we for example want to rotate the state $|0\rangle$ to $|1\rangle$, we can make use of the Pauli X-matrix

$$X|0\rangle = |1\rangle \iff \begin{pmatrix} 0 & 1 \\ 1 & 0 \end{pmatrix} \begin{pmatrix} 1 \\ 0 \end{pmatrix} = \begin{pmatrix} 0 \\ 1 \end{pmatrix}. \tag{1.14}$$

The operation, depicted in figure 1.3 using quantum circuit notation, involves the representation of qubits as lines upon which gates are applied. In the context of quantum circuits, a quantum register serves as a collection of qubits, collectively manipulated during the computation. Gates, representing quantum operations, act on these qubits, influencing their quantum states. It is crucial to note that a quantum circuit is always ended by a measurement gate. This gate performs a projection onto the basis states $|0\rangle$ and $|1\rangle$, yielding measurement outcomes. In quantum circuits, measurements provide classical information and play a pivotal role in extracting results from quantum computations.

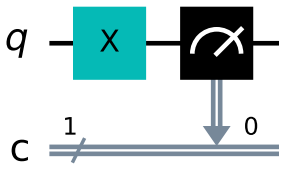

Figure 1.3: Simple circuit to rotate an initial state vector by π radians around the x-axis using the X operator. Note, this circuit has a classical register that is used to map the outcome of the qubit to a classical bit. The picture was generated using qutip [8].

The X-gate is an example of a single-qubit gate and a straight forward generalization can be done by considering a general initial state

$$|\psi\rangle = \alpha|0\rangle + \beta|1\rangle, \tag{1.15}$$

then single-qubit gates are simple 2x2 matrices, with

$$|\psi_{new}\rangle = \mathbf{M}\,|\psi_{old}\rangle\,, \tag{1.16}$$

where the unitary matrices are equivalent to considered quantum gates.
Following is a list of the most important single-qubit gates.

- Hadamard (is a rotation of the sphere about the y-axis by 90°, followed by a rotation about the x-axis by 180°)

$$\mathbf{H} = \frac{1}{\sqrt{2}}\begin{bmatrix}1 & 1\\ 1 & -1\end{bmatrix} \tag{1.17}$$

- Pauli-X (quantum not gate, 180° rotation around x-axis)

$$\mathbf{X} = \begin{bmatrix}0 & 1\\ 1 & 0\end{bmatrix} \tag{1.18}$$

- Pauli-Y (180° rotation around y-axis)

$$\mathbf{Y} = \begin{bmatrix}0 & -i\\ i & 0\end{bmatrix} \tag{1.19}$$

- Pauli-Z (180° rotation around z-axis)

$$\mathbf{Z} = \begin{bmatrix}1 & 0\\ 0 & -1\end{bmatrix} \tag{1.20}$$

- Phase (90° rotation around z-axis)

$$\mathbf{S} = \begin{bmatrix}1 & 0\\ 0 & i\end{bmatrix} \tag{1.21}$$

- $\pi/8$ (45° rotation around z-axis)

$$\mathbf{T} = \begin{bmatrix}1 & 0\\ 0 & e^{i\pi/4}\end{bmatrix} \tag{1.22}$$

Another important quantum gate is the controlled-not (CNOT or CX) gate. It is different from the preceding gates in that it is acting on two-qubits, therefore

referred to as a two-qubit gate,

$$\mathbf{CX} = \begin{bmatrix} 1 & 0 & 0 & 0 \\ 0 & 1 & 0 & 0 \\ 0 & 0 & 0 & 1 \\ 0 & 0 & 1 & 0 \end{bmatrix}. \tag{1.23}$$

It is made up of a target and a control qubit and basically it applies a X-gate onto the target qubit whenever the control qubit is in the $|1\rangle$ state, otherwise leaving the target qubit unchanged. This gate in particular is important since it can be shown that any two-qubit gate can be derived from a universal single-qubit gate set plus the CNOT gate [7]. By a universal gate set, we mean a set of all possible rotations on the Bloch sphere. This is achieved by e.g. the Hadamard **H**, the **S** and the **T** gates or more generally by the three rotation gates [10]

$$\mathbf{R}_x = \begin{bmatrix} \cos(\theta/2) & -i\sin(\theta/2) \\ -i\sin(\theta/2) & \cos(\theta/2) \end{bmatrix}, \tag{1.24}$$

$$\mathbf{R}_y = \begin{bmatrix} \cos(\theta/2) & -\sin(\theta/2) \\ \sin(\theta/2) & \cos(\theta/2) \end{bmatrix}, \tag{1.25}$$

$$\mathbf{R}_z = \begin{bmatrix} e^{-i\theta/2} & 0 \\ 0 & e^{i\theta/2} \end{bmatrix}. \tag{1.26}$$

1.4 Quantum operations

As we discussed before, quantum states transform using unitaries. These are operations that 1) preserve probability and 2) are linear maps,

$$|\psi'\rangle = U\,|\psi\rangle\,. \tag{1.27}$$

Different from what we considered before, we can also transform a quantum state within the density matrix formalism. The connection between the two formalisms

is straight forward using the definition of the density matrix

$$\rho' = \sum_{k=1}^{l} p_k \left|\psi'_k\right\rangle \left\langle\psi'_k\right| = \sum_{k=1}^{l} p_k U \left|\psi_k\right\rangle \left\langle\psi_k\right| U^\dagger \tag{1.28}$$

$$= U\rho U^\dagger. \tag{1.29}$$

A generalization of this is done by introducing the quantum operation [7, 11]. We want to describe the unitary evolution of a system with its environment. To do this, we assume that the two subsystems are not entangled and that the environment is initially in a pure state. Since we are only interested in the reduced density matrix of our subsystem, we will use the partial trace to ignore the environment after the transformation

$$\rho' = \mathrm{Tr}_B \left[U(\rho \otimes \rho_B)U^\dagger\right] \tag{1.30}$$

$$= \mathrm{Tr}_B \left[U(\rho \otimes \left|\psi\right\rangle_B \left\langle\psi\right|_B U^\dagger\right] \tag{1.31}$$

$$= \sum_k {}_B\langle k|U\left|\psi\right\rangle_B \ \rho \ {}_B\langle\psi|U^\dagger\left|k\right\rangle_B, \tag{1.32}$$

with B referring to the environment and ρ the system's density matrix. At this point, we can define the operators $E_k = {}_B\langle k|U\left|\psi\right\rangle_B$, so

$$\epsilon(\rho) = \sum_k E_k \rho E_k^\dagger, \tag{1.33}$$

with $\mathrm{Tr}(\epsilon(\rho)) = 1$. This mapping is called a operator-sum of Kraus operators E_k which satisfy $\sum_k E_k^\dagger E_k = 1$. So in general, we introduce a transformation

$$\rho' = \epsilon(\rho), \tag{1.34}$$

where for now, we have made the reasonable assumption that the initial composite state starts out in a pure product state.
The introduced map $\epsilon : \rho \to \rho'$ that has the following properties,

1. linear;
2. preserves hermiticity;
3. trace preserving;

4. completely positive: if $\rho \geq 0$ then $\epsilon(\rho) \geq 0$.

1.5 Noise channels

We can represent noise channels as quantum operations inside a circuit, in which the environment is represented by qubits. In this respect, a quantum noise channel $E(\rho)$ on the system maps the initial quantum state of the system to the final state after an interaction with the environment.
Let us consider a 3-qubit system, where the environment is represented by 2 qubits and the system by the third qubit [11]. Initially, the environment is in the pure state

$$|\psi_{env}\rangle = \alpha\,|00\rangle + \beta\,|01\rangle + \gamma\,|10\rangle + \delta\,|11\rangle\,. \tag{1.35}$$

We now examine a transformation as implemented in figure 1.4,

$$\mathbf{U} = \begin{bmatrix} \sigma_x & 0 & 0 & 0 \\ 0 & \sigma_y & 0 & 0 \\ 0 & 0 & \sigma_z & 0 \\ 0 & 0 & 0 & I \end{bmatrix}. \tag{1.36}$$

Note, subsequently we use both notations, e.g. $\sigma_x = X$, for the Pauli matrices interchangeably.

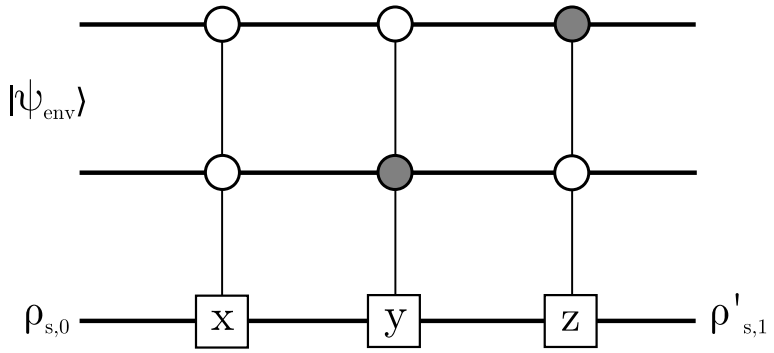

Figure 1.4: Qualitative picture of a general noise channel. White circles represent $|0\rangle$ and grey circles $|1\rangle$. (Inspired by [11].)

Initially, we have the total density matrix as given by

$$\rho_{tot,0} = |\psi_{env}\rangle\langle\psi_{env}| \otimes \rho_{s,0} \begin{bmatrix} |\alpha|^2\rho_s & 0 & 0 & 0 \\ 0 & |\beta|^2\rho_s & 0 & 0 \\ 0 & 0 & |\gamma|^2\rho_s & 0 \\ 0 & 0 & 0 & |\delta|^2\rho_s \end{bmatrix}, \tag{1.37}$$

where the 0s denote matrices of zeros and ρ_s is our systems density matrix. After the considered operation we obtain

$$\rho_{tot,1} = \mathbf{U}\rho_{tot,0}\mathbf{U}^\dagger. \tag{1.38}$$

To obtain the final state of the system, we trace over the environment

$$\begin{aligned} \rho'_{s,1} =& \mathrm{Tr}_{env}(\rho_{tot,1}) && (1.39)\\ =& |\alpha|^2\sigma_x\rho_s\sigma_x^\dagger + |\beta|^2\sigma_y\rho_s\sigma_y^\dagger + |\gamma|^2\sigma_z\rho_s\sigma_z^\dagger + |\delta|^2\rho_s. && (1.40) \end{aligned}$$

We can cast this to an operator sum representation by rewriting the expression as

$$\rho'_{s,1} = \sum_{i=0}^{3} E_i\rho_s E_i^\dagger. \tag{1.41}$$

With this depiction we have achieved a quantum circuit that implements the X-gate when the environment is in the state $|00\rangle$, the Y-gate when in state $|01\rangle$, the Z-gate when in $|10\rangle$ and the identity when in $|11\rangle$. All the noise channels that will be studied in this work can be derived from this simple picture by explicitly choosing the parameters α, β, γ and δ plus the normalization condition $|\alpha|^2+|\beta|^2+|\gamma|^2+|\delta|^2 = 1$.
In the following we directly use the Kraus operators used in the operator sum representation, which are

$$E_0 = |\delta|I,\ E_1 = |\alpha|\sigma_x,\ E_2 = |\beta|\sigma_y,\ E_3 = |\gamma|\sigma_z. \tag{1.42}$$

Starting from this general expression, we will derive the channels for depolarization, pure dephasing and amplitude damping [7]. The **Depolarization channel** drives the system towards the totally mixed one and therefore is given by setting $|\alpha|^2, |\beta|^2$

and $|\gamma|^2$ to $p/3$, where p is the probability to depolarize. Thus,

$$E_0 = I\sqrt{1-p},\ E_1 = \sigma_x\sqrt{\frac{1}{3}p},\ E_2 = \sigma_y\sqrt{\frac{1}{3}p},\ E_3 = \sigma_z\sqrt{\frac{1}{3}p}, \tag{1.43}$$

or written out

$$\rho_{new} = \frac{1}{3}p\left[\sigma_x\rho\sigma_x^\dagger + \sigma_y\rho\sigma_y^\dagger + \sigma_z\rho\sigma_z^\dagger\right] + (1-p)\rho. \tag{1.44}$$

In terms of the Bloch sphere, this achieves a "shrinking" of the sphere with the center always at the origin (totally mixed state), as can be seen in figure 1.5a. It is possible to recast the result as a time evolution, by considering the probability of depolarization in terms of time and including a decay constant.
We assume that the probability to depolarize is $p = 1 - e^{-\frac{t}{T_p}}$. With this, we get to the transformation

$$\epsilon(\rho) = \frac{1}{3}(1-e^{-\frac{t}{T_p}})\left[\sigma_x\rho\sigma_x^\dagger + \sigma_y\rho\sigma_y^\dagger + \sigma_z\rho\sigma_z^\dagger\right] + (1-1+e^{-\frac{t}{T_p}})\rho, \tag{1.45}$$

where we expand the exponential in a series up to first order (we require $T_p \gg t_g$, where t_g is the time we apply the gate) and we replace t with an infinitesimal time-step dt. Then we get the expression

$$\begin{aligned}
\rho(t+dt) &= \frac{1}{3}\frac{dt}{T_p}\left[\sigma_x\rho\sigma_x^\dagger + \sigma_y\rho\sigma_y^\dagger + \sigma_z\rho\sigma_z^\dagger\right] + (1-\frac{dt}{T_p})\rho \\
\rightarrow \frac{\rho(t+dt)+\rho(t)}{dt} &= \frac{1}{3}\frac{1}{T_p}\left[\sigma_x\rho\sigma_x^\dagger + \sigma_y\rho\sigma_y^\dagger + \sigma_z\rho\sigma_z^\dagger\right] - \frac{1}{T_p}\rho \\
&\rightarrow \dot{\rho} = \frac{\gamma_d}{3}\sum_{k=1}^{3}\left[\sigma_k\rho\sigma_k - \rho\right],
\end{aligned} \tag{1.46}$$

with $\sigma_x = \sigma_1$ etc.
Note, it is instructive to make the change of variables $s = t/t_g$, $dt = t_g ds$, to get dimensionless time-steps.
The **Amplitude damping channel** is achieved by setting $|\alpha| = \sqrt{p}$, $|\beta| = 0$, $\gamma = 0$ and $|\delta| = \sqrt{1-p}$. It drives the system towards the ground state $|0\rangle$ and arises from the interaction with the surrounding environment, e.g. the drive to thermal equilibrium. It can also arise from control and measurement faults,

Writing the matrices out

$$\begin{aligned}\rho_{new} &= E_0\rho E_0^\dagger + E_1\rho E_1^\dagger \\ &= \begin{bmatrix}1 & 0\\ 0 & \sqrt{1-p_1}\end{bmatrix}\begin{bmatrix}\rho_{00} & \rho_{01}\\ \rho_{10} & \rho_{11}\end{bmatrix}\begin{bmatrix}1 & 0\\ 0 & \sqrt{1-p_1}\end{bmatrix} + \\ &\quad \begin{bmatrix}0 & \sqrt{p_1}\\ 0 & 0\end{bmatrix}\begin{bmatrix}\rho_{00} & \rho_{01}\\ \rho_{10} & \rho_{11}\end{bmatrix}\begin{bmatrix}0 & 0\\ \sqrt{p_1} & 0\end{bmatrix} \\ &= \begin{bmatrix}\rho_{00}+p_1\rho_{11} & \sqrt{1-p_1}\rho_{01}\\ \sqrt{1-p_1}\rho_{10} & (1-p_1)\rho_{11}\end{bmatrix}.\end{aligned} \tag{1.47}$$

It is represented in figure 1.5b.

Pure dephasing, equivalent to a phase-flip channel, on the other hand is attained by setting $|\alpha| = |\beta| = 0$. It is purely quantum mechanical, in the sense that it only affects the loss of coherence without the loss of energy. In that case we obtain

$$\rho_{new} = p_z\sigma_z\rho\sigma_z^\dagger + (1-p_z)\rho \tag{1.48}$$

$$= p_z(Z\rho Z - \rho) + \rho, \tag{1.49}$$

with $|\gamma|^2 = p_z$ the probability of phase-flipping. Effectively this achieves a deformation of the Bloch sphere to an ellipsoid with the Z-axis its long side's center. This can also be seen in figure 1.5c.

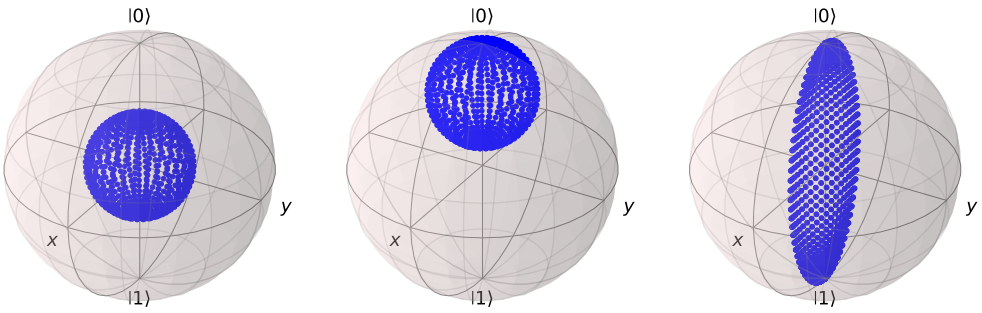

(a) Depolarization **(b)** Amplitude damping **(c)** Dephasing

Figure 1.5: Noise channels that are considered in this work and their effects on the state vector visualized as a Bloch sphere. Note, the grey Bloch sphere represents no noise channel and the blue Bloch sphere the effect of the considered noise channel on the available states.

2

Noisy gate derivation

In this section, we show how we can incorporate the non-unitary dynamics of interactions with the environment into the gate formalism. By integrating stochastic and deterministic noise into the logical gate, we replace the exact gate with the noisy alternative. Starting point is the stochastic Schrödinger equation.

2.1 Time-evolution of open systems

In order to describe the continuous temporal evolution of open quantum systems, it is convenient to first recast the Schrödinger equation in the density matrix formalism via the von Neumann equation

$$\frac{\partial \rho(t)}{\partial t} = -\frac{i}{\hbar}[H_{tot}, \rho(t)], \tag{2.1}$$

where in general the Hamiltonian includes environment and environment-system interaction effects,

$$H_{tot} = H + H_{env} + H_{int}. \tag{2.2}$$

An open system is a quantum system S coupled to another quantum system E, called environment. While it is usually assumed that the combined total system

$S + E$ is closed, the state of the subsystem S is subjected to its internal dynamics and to the interaction with the environment. The interaction leads to certain system-environment correlations and in general the reduced system S dynamics cannot be represented in terms of unitary, Hamiltonian dynamics.
The reduced density matrix at time t is obtained from the density matrix of the total system by tracing out the degrees of freedom of the environment. If the evolution of the total system $S + E$ is closed, then the equation of motion for the reduced density matrix is obtained by taking the partial trace over the environment on both sides of the von Neumann equation, 2.1, ending up with

$$\frac{\partial \rho_S(t)}{\partial t} = -\frac{i}{\hbar}\mathrm{Tr_E}\left\{[H_{tot}, \rho(t)]\right\}, \tag{2.3}$$

which is the starting point for deriving an equation for the system state alone, that yields a non unitary evolution. Equations of this type are called master equations and generally assume markovity, meaning the time derivative of the system's density matrix depends only on the density matrix at the current time and not on the density matrix at previous times. Master equations are written as

$$\frac{\partial \rho(t)}{\partial t} = \mathcal{L}\left[\rho(t)\right], \tag{2.4}$$

with $\mathcal{L}$ the generator of both the unitary and the dissipative, non-unitary dynamics and here, we drop the subscript S to describe the density matrix of the system.
To continue, we also usually work within the Born approximation (system and environment only interact weakly) and we assume that the system and the environment were uncorrelated before the interaction was turned on.
Within the framework of quantum operations, master equations are generally called Lindblad master equations, where the generator has the form

$$\mathcal{L}(\rho) = -\frac{i}{\hbar}\left[H, \rho\right] + \mathcal{D}(\rho) = i\hbar[H, \rho] + \sum_i L_i^\dagger \rho L_i - \frac{1}{2}(L_i^\dagger L_i \rho + \rho L_i^\dagger L_i). \tag{2.5}$$

The Lindblad operators L_i can be derived from the the previously defined noise channels, eqs. 1.44, 1.47 and 1.48. To see the correspondence, consider a noise

contribution from pure dephasing,

$$\rho_{new} = p_z(\sigma_z \rho \sigma_z - \rho) + \rho. \tag{2.6}$$

We assume the probability of dephasing to be $p_z = 1 - e^{-\frac{t}{T_z}}$, then

$$\rho(t + dt) - \rho(t) = \left(1 - e^{-\frac{t}{T_z}}\right)(\sigma_z \rho(t) \sigma_z - \rho(t)). \tag{2.7}$$

If we, like before, expand the exponential series up to first order and replace t with an infinitesimal time-step dt, we end up with

$$\frac{\rho(t + dt) - \rho(t)}{dt} = \gamma_z (\sigma_z \rho(t) \sigma_z - \rho(t)). \tag{2.8}$$

Since the Pauli matrices are both hermitian and unitary we can immediately rewrite the expression in the limit $dt \to 0$, as

$$\dot{\rho} = L_z^\dagger \rho L_z - \frac{1}{2}(L_z^\dagger L_z \rho + \rho L_z^\dagger L_z), \tag{2.9}$$

where $L_z = \sqrt{\gamma_z}\sigma_z$ is the Lindblad operator for pure dephasing.
With this, we have a way to describe the non-unitary dynamics of our system as an evolution that has a unitary contribution and the Lindblad operators, which describe the effect of the environment. For a particular system, we now have to 1) find the Hamiltonian that governs the unitary dynamics and 2) the Lindblad operators L_i that generate the non-unitary dynamics.
It is possible to unravel the master equation 2.4, obtaining a stochastic Schrödinger equation [12]

$$d|\psi\rangle = \left[-\frac{i}{\hbar} H dt + \sum_{k=1} [i\, dW_{k,t} L_k - \frac{1}{2} dt L_k^\dagger L_k]\right] |\psi\rangle, \tag{2.10}$$

where $dW(t)$ is a Gaussian stochastic variable and referred to as the Wiener measure.
In general, we can assume that the mixedness of the density matrix is the result of an average of several possible pure states $|\psi\rangle$. Each of these states is associated with a probability P, reflecting the likelihood of the system being in a specific pure

state. Therefore, solutions of stochastic Schrödinger equations are usually called quantum trajectories and are defined and can be addressed within the framework of Ito stochastic calculus [13]. Lastly, we again recover an unbiased estimator of the density matrix by averaging over the trajectories over the pure states $|\psi\rangle$. The point of doing this unraveling is to derive an expression that can be used to manipulate the state vector itself. We can then simply replace the previously defined unitary gate acting on our state with the corresponding non-unitary noisy gate.

2.2 Noisy gates

This section and section 2.3 follow the previously mentioned article [6].
Usually, modelling noise in gate-based systems is done by including appropriate noise channels acting before and after the unitary gate [11], i.e. by trotterizing the evolution and the error . This approximation is justified, since the used gate times t_g are much smaller than the characteristic times of considered decoherence effects. Instead, a more detailed description can be obtained by integrating the noise into the gates themselves, so to solve the dynamics that the system coupled with the environment generate during a gate. The novel description offers a more detailed description and therefore is expected to yield a more accurate circuit simulations, thereby helping to understand in more detail how different noises modify the ideal gate dynamics.

2.3 General derivation of noisy gates

We start by writing the Lindblad term in terms of the dimensionless parameter ϵ

$$\mathcal{D}(\rho) = \epsilon^2 \sum_{k=1} \left[L_k \rho L_k^\dagger - \frac{1}{2} \left\{ L_k^\dagger L_k, \rho \right\} \right], \tag{2.11}$$

where $\epsilon = \sqrt{\gamma_{tot}}$ is the sum of all characteristic decay rates normalized by the gate time t_g for the considered noise contributions. The characteristic time scales are given by $1/\gamma_i = T_i/t_g$, with T_i the specific relaxation time. The assumption we revisit here is that the typical order of magnitude of the time to execute any

gate is multiple orders lower than the typical order of magnitude of the considered decoherence times, meaning $\epsilon \ll 1$.
We continue by writing the stochastic Schrödinger equation with this newly introduced parameter

$$d\left|\psi_s\right\rangle = \left[-\frac{i}{\hbar}H_s ds + \sum_{k=1}^{N^2-1}\left[i\epsilon\, dW_{k,s}L_k - \frac{\epsilon^2}{2}dsL_k^\dagger L_k\right]\right]\left|\psi_s\right\rangle . \tag{2.12}$$

Here, we see why it is crucial to introduce the parameter ϵ. We can solve eq. 2.12 approximately with the solution in the order of $\mathcal{O}(\epsilon^2)$, using a perturbative approach for ϵ. This is valid with the assumptions we made, i.e. that we work within the small noise expansion.
For simplicity, we consider only the $k = 1$ term, while the generalization to more terms can be done straight forwardly,

$$d\left|\psi_s\right\rangle = \left[-\frac{i}{\hbar}H_s ds + \left[i\epsilon dW_{1,s}L_1 - \frac{\epsilon^2}{2}dsL_1^\dagger L_1\right]\right]\left|\psi_s\right\rangle , \tag{2.13}$$

and we use a perturbative Ansatz of the form

$$\left|\psi_s\right\rangle = \left|\psi_s^0\right\rangle + \epsilon\left|\psi_s^1\right\rangle + \epsilon^2\left|\psi_s^2\right\rangle + \mathcal{O}(\epsilon^3). \tag{2.14}$$

As usual, we put the Ansatz into the SDE and associate terms with same powers of ϵ. Then we get the following system of SDEs

$$d\left|\psi_s^0\right\rangle = -\frac{i}{\hbar}H_s\left|\psi_s^0\right\rangle ds \tag{2.15}$$

$$d\left|\psi_s^1\right\rangle = -\frac{i}{\hbar}H_s\left|\psi_s^1\right\rangle ds + iL_1\left|\psi_s^0\right\rangle dW_{1,s} \tag{2.16}$$

$$d\left|\psi_s^2\right\rangle = -\frac{i}{\hbar}H_s\left|\psi_s^2\right\rangle ds + iL_1\left|\psi_s^1\right\rangle dW_{1,s} - \frac{1}{2}L_1^\dagger L_1\left|\psi_s^0\right\rangle ds, \tag{2.17}$$

with initial condition $\left|\psi_0^0\right\rangle = \left|\psi_0\right\rangle$.
The solution to the zeroth order is

$$\left|\psi_s^0\right\rangle = U_s\left|\psi_0\right\rangle , \tag{2.18}$$

with $U_s = e^{-\frac{i}{\hbar}H_s}$. The first order is an Ornstein-Uhlenbeck process and the solution can be found by first rearranging the SDE and plugging the zeroth order solution in

$$d\left|\psi_s^1\right\rangle + \frac{i}{\hbar}H_s\left|\psi_s^1\right\rangle ds = iL_1U_s\left|\psi_0\right\rangle dW_{1,s}, \tag{2.19}$$

then multiplying by an integration factor, in this case U_s, and integrating both sides, using the property $\left[U_s d\left|\psi_s^1\right\rangle + \frac{i}{\hbar}H_sU_s\left|\psi_s^1\right\rangle ds\right] = d\left[U_s\left|\psi_s^1\right\rangle\right]$,

$$U_s\left[d\left|\psi_s^1\right\rangle + \frac{i}{\hbar}H_s\left|\psi_s^1\right\rangle ds\right] = U_siL_1U_s\left|\psi_s^0\right\rangle dW_{1,s} \tag{2.20}$$

$$\rightarrow \int d\left[U_s\left|\psi_s^1\right\rangle\right] = \int U_siLU_s\left|\psi_0\right\rangle dW_s. \tag{2.21}$$

Now, we define $S_s = \int_0^s dW_\tau L_\tau$ and we use the unitary property of the gate $U_s^\dagger U_s = 1$ and that $\left|\psi_0^1\right\rangle = 0$, we end up with

$$\left|\psi_s^1\right\rangle = iU_sS_s\left|\psi_0\right\rangle. \tag{2.22}$$

For the second order SDE we essentially use the same procedure to find the solution

$$\left|\psi_s^2\right\rangle = -U_s\int_0^s\left[\frac{1}{2}L_s^\dagger L_s ds + L_sS_s dW_s\right]\left|\psi_0\right\rangle, \tag{2.23}$$

with $L_s = U_s^\dagger L_1 U_s$.
Now, the final approximate solution can be constructed,

$$\left|\psi_{s=1}\right\rangle = U_gN\left|\psi_0\right\rangle + \mathcal{O}(\epsilon^3), \tag{2.24}$$

with $U_g = U_{s=1}$ and

$$N = \left[1 + \epsilon S_1 - \epsilon^2\int_0^1\left[\frac{1}{2}L_s^\dagger L_s ds + L_sS_sW_s\right]\right], \tag{2.25}$$

which can be rewritten using Itos rule (the equivalent of the chain rule in stochastic calculus [13])

$$\int_0^\tau dW_s L_s S_s = \frac{1}{2}\left[S_s^2 + \int_0^\tau dW_s[L_s, S_s] - \int_0^\tau ds L_s^2\right]. \tag{2.26}$$

Then,

$$N = 1 + i\epsilon S_1 - \frac{\epsilon^2}{2}\left[S_1^2 + \int_0^1 ds[L_s^\dagger - L_s]L_s + \mathcal{C}\right], \tag{2.27}$$

which are the first terms of a series expansion of an exponential

$$e^\Xi = 1 + i\epsilon S_1 - \frac{\epsilon^2}{2}S_1^2 + \mathcal{O}(\epsilon^3), \tag{2.28}$$

$$e^\Lambda = 1 - \frac{\epsilon^2}{2}\left(\int_0^1 ds[L_s^\dagger - L_s]L_s + \mathcal{C}\right) + \mathcal{O}(\epsilon^4) \tag{2.29}$$

Therefore

$$N = e^\Lambda e^\Xi + \mathcal{O}(\epsilon^3), \tag{2.30}$$

where we have one deterministic and one stochastic term

$$\Lambda = -\frac{\epsilon^2}{2}\int_0^1 ds \sum_{k=1}^{N^2-1}[L_{k,s}^\dagger L_{k,s} - L_{k,s}^2] \tag{2.31}$$

$$\Xi = i\epsilon \sum_{k=1}^{N^2-1}\int_0^1 dW_{k,s} L_{k,s}, \tag{2.32}$$

where it is important to remember that, from before, the Lindblad operators are written in the interaction picture, i.e. $L_{k,s} = U_s^\dagger L_k U_s$.
On top of that, we redefine the stochastic part in terms of random variables

$$\Xi_{ij} = i\epsilon \sum_{k=1}^{N^2-1}[\xi_{kij}^+ + i\xi_{kij}^-], \tag{2.33}$$

with $L_{kij,s} = L^+_{kij,s} + iL^-_{kij,s}$ the entries of each matrix entry written in terms of real and imaginary part and we defined the Ito integrals

$$\xi^+_{kij} = \int_0^1 dW_{k,s} L^+_{kij,s} \tag{2.34}$$

$$\xi^-_{kij} = \int_0^1 dW_{k,s} L^-_{kij,s}, \tag{2.35}$$

which are Ito integrals of non anticipating functions and therefore follow standard rules, normally distributed with zero mean and correlated by

$$\left\langle \xi^+_{kij} \xi^-_{kij} \right\rangle = \int_0^1 ds L^+_{kij,s} L^-_{ki'j',s}. \tag{2.36}$$

Finally, we have defined everything we need to implement the gates. If we know the type of operation, i.e. the Hamiltonian. We can then evaluate the stochastic and deterministic term separately, exponentiate and multiply with the noiseless gate U_g to get the noisy version.

3

Superconducting qubits

In this chapter, we first introduce the basic concepts of the superconducting qubit, derive the implemented single- and two-qubit unitaries and then discuss the relevant noise in this hardware. Finally, we show the performance of the noisy gates algorithm applied to this architecture as compared to the exact solution. To this aim we implement the noisy gates protocol in a Python code that performs the noisy gate, when supplied with a Hamiltonian, the different noise terms in the interaction picture, the covariance matrices of the Wiener integrals and an initial state vector.

3.1 Quantum LC circuit

The superconducting qubit is essentially an LC circuit, where the inductor is replaced by a Josephson junction. Therefore, it is instructive to start with a quantum mechanical treatment of the LC circuit.
The energy stored by the capacitor in an LC circuit is

$$U_C = \frac{1}{2}CV^2 = \frac{Q^2}{2C}, \tag{3.1}$$

with C the capacitance, V the voltage and the circuit charge defined as

$$Q = \int_{-\infty}^{t} I(t')dt'. \tag{3.2}$$

The energy stored in the inductor, on the other hand, is

$$U_L = \frac{1}{2}LI^2 = \frac{\Phi^2}{2L}, \tag{3.3}$$

with inductance L and the flux defined as

$$\Phi = \int_{-\infty}^{t} V(t')dt'. \tag{3.4}$$

We define the flux as the canonical coordinate in the Lagrangian

$$\mathcal{L} = \mathcal{T} - \mathcal{U} \tag{3.5}$$

$$= U_C - U_L = \frac{1}{2}C\dot{\Phi}^2 - \frac{\Phi^2}{2L} \tag{3.6}$$

Then the conjugate momentum of the flux is

$$\frac{\partial \mathcal{L}}{\partial \dot{\Phi}} = C\dot{\Phi} = Q, \tag{3.7}$$

by the definition of the circuit charge variable.
The corresponding Hamiltonian of this system is

$$H = Q\dot{\Phi} - \mathcal{L} \tag{3.8}$$

$$= \frac{1}{2}C\dot{\Phi}^2 + \frac{\Phi^2}{2L} = \frac{Q^2}{2C} + \frac{\Phi^2}{2L}. \tag{3.9}$$

We can rewrite this in a more instructive form by recalling that

$$\omega = \sqrt{\frac{1}{LC}}, \tag{3.10}$$

then

$$H = \frac{Q^2}{2C} + C\frac{\omega^2}{2}\Phi^2. \tag{3.11}$$

as compared to the well known Hamiltonian for the harmonic oscillator [14]

$$H = \frac{p^2}{2m} + m\frac{\omega^2}{2}x^2, \tag{3.12}$$

where the canonical variables are exchanged and the mass m replaces the capacitance.
For the purpose of having a quantum mechanical description of the system, we have to promote the charge and flux coordinate to quantum mechanical operators obeying the commutation relation [15]

$$[\hat{\Phi}, \hat{Q}] = i\hbar. \tag{3.13}$$

For simplicity, however, we drop the hat of the operators in the subsequent treatment.
It is convenient to introduce the reduced flux and reduced charge variables,

$$\phi = 2\pi\frac{\Phi}{\Phi_0}, \tag{3.14}$$

$$n = \frac{Q}{2q_e}, \tag{3.15}$$

where we defined the superconducting magnetic flux quantum as $\Phi_0 = h/2q_e$.
Using the reduced quantities, we rewrite the quantum mechanical LC Hamiltonian as

$$H = 4E_C n^2 + \frac{1}{2}E_L\phi^2, \tag{3.16}$$

where $E_C = q_e^2/2C$ is the charging energy and $E_L = (\Phi_0/2\pi)^2/L$ the inductive energy. To summarize, the obtained Hamiltonian, 3.16, describes a resonant circuit

which has equally spaced energy levels, whose spacing is given by

$$\Delta E = \hbar\omega_r = \frac{\hbar}{\sqrt{LC}} = \sqrt{8E_C E_L}. \tag{3.17}$$

If we intend to encode quantum information, we need the levels to not be equally spaced, so we introduce an anharmonicity in the circuit. Then, we can target and encode information in specific states which, in the case of charge qubit, correspond to the discrete charge levels (excess in the Cooper pairs) on the superconducting island, namely the superconducting section of the circuit between the capacitor and the junction.
The nonlinear inductor placed instead of the linear one is called Josephson junction, and is made up of two superconductors separated by a thin insulating layer. The nonlinear behaviour stems from the fact that, if the layer is thin enough, discrete charges can tunnel through the barrier.
The extension of the quantum LC Hamiltonian to the Josephson junction Hamiltonian is straight forward using the Josephson equations [16] (we derive them in Appendix A.1)

$$I = I_c \sin(\phi), \tag{3.18}$$

$$V = \frac{\Phi_0}{2\pi}\frac{\partial\phi}{\partial t}. \tag{3.19}$$

where I_c is the (critical) maximum current that can flow inside the junction. The modified Hamiltonian is then [15]

$$H = 4E_C n^2 - E_J \cos(\phi), \tag{3.20}$$

where $E_J = I_C\Phi_0/2\pi$ is the Josephson energy. At this point, we can compare the two findings. We evaluate the two Hamiltonians and determine the respective wave functions and energies for the first few levels, as can be seen in figure 3.1.

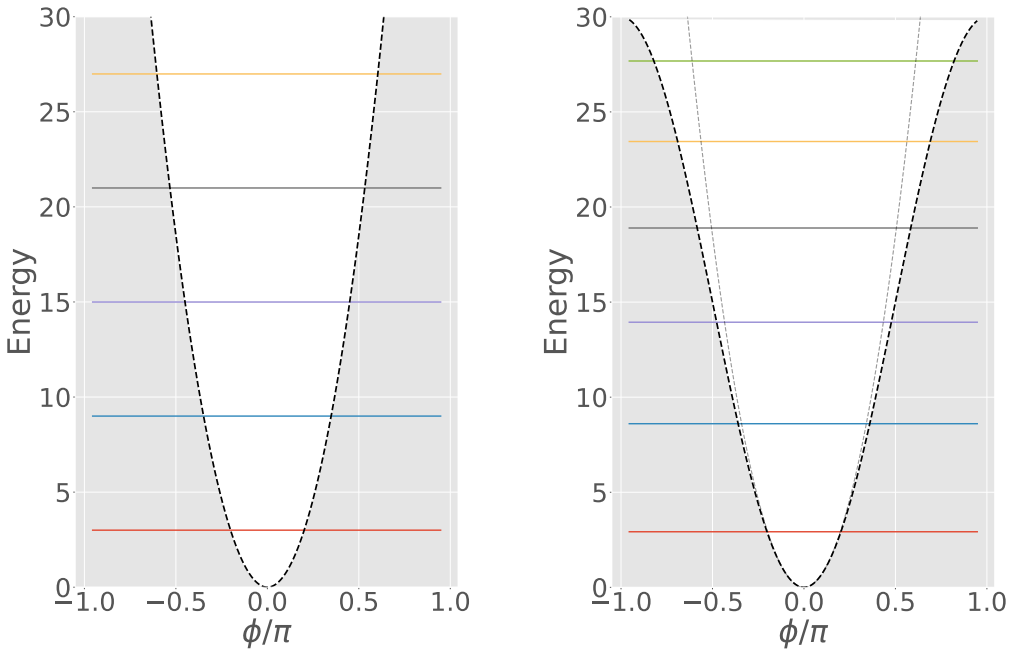

(a) Normal QHO: $H = 4E_C n^2 + \frac{1}{2}E_L\phi^2$ **(b)** SC qubit: $H = 4E_C n^2 - E_J\cos(\phi)$

Figure 3.1: In this example we set $E_C = 0.3$ and $E_L = E_J = 15$ and we show the first few low lying energy levels for the two types of potentials. For (a) the quantum harmonic oscillator, the energy levels are equally spaced with $\Delta E = \sqrt{8E_C E_L} = 6$. In (b), we see that the energy difference of adjacent levels gets smaller as you climb up the energy levels. The solutions were obtained by finite differences, note we shifted along y such that both solutions start at 0.

The LC Hamiltonian 3.16 has a parabolic potential, from which the harmonic spectrum originates. After introducing the Josephson junction, the parabolic potential is replaced by a cosinusoidal one, whose energy spectrum now is anharmonic. For the charge qubit, the electrostatic energy of the Cooper-pair on the superconducting island is larger than the Josephson coupling energy on the junction, i.e. $E_J \ll E_C$. The relevant quantum variable is the number of Cooper pairs that cross Josephson junction. By writing the Hamiltonian 3.20 in the charge basis highlights the coupling between consecutive charge levels

$$H = \sum_n [E_C(n - n_g)^2|n\rangle\langle n| E_J(|n\rangle\langle n+1| + |n+1\rangle\langle n|)], \tag{3.21}$$

where $n_g = CV/2e$ is the number of induced Cooper pairs on the capacitor. The ratio E_J/E_C tunes the sensitivity of the qubit toward the charge noise: In this

setup, the charge dispersion decreases exponentially in E_J/E_C , while the anharmonicity decreases with a slow power law of E_J/E_C, allowing for a workable effective two-level system. We will discuss the relevant noises in the charge qubit in chapter 3.4.

3.2 Single-qubit gate

Here, we review a technique for driving single-qubit gates and certain two-qubit gates with the SC qubit that is based on the capacitive coupling of a microwave line to the qubit [15]. The technique we introduce is applicable to all types of superconducting qubits, even though we refer specifically to the charge qubit, such as the Cooper-pair box and transmon-like qubits. To demonstrate the capability of driving single-qubit gates, we consider coupling a superconducting qubit to a microwave source (or qubit drive) as shown in Figure 3.2.

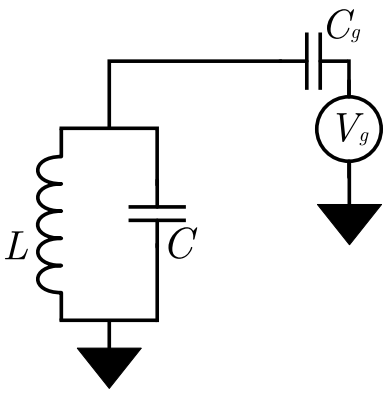

Figure 3.2: Circuit diagram of a Cooper pair box - here, represented as a Josephson junction L in parallel with a capacitor C - capacitively (C_g) coupled to a microwave drive line, characterized by a time-dependent voltage V_g.

For the Cooper pair box, the energy stored by the inductor is as before

$$U_L = \frac{1}{2}LI^2 = \frac{\phi^2}{2L}. \tag{3.22}$$

The energy stored by the capacitor in the LC circuit is also again

$$U_C = \frac{1}{2}CV^2 = \frac{1}{2}C\dot{\phi}^2, \tag{3.23}$$

and by the capacitor in parallel with the junction

$$U_{C_g} = \frac{1}{2}C_g(V - V_g)^2 = \frac{1}{2}C_g(\dot{\phi} - V_g)^2. \tag{3.24}$$

The corresponding Lagrangian is thus

$$\mathcal{L} = \mathcal{T} - \mathcal{U} = \frac{1}{2}C\dot{\phi}^2 - \frac{1}{2L}\phi^2 + \frac{1}{2}C_g(\dot{\phi} - V_g)^2, \tag{3.25}$$

where the flux ϕ is again identified as the canonical coordinate. From this we get the Hamiltonian

$$H_{LC} = Q\dot{\phi} - \mathcal{L} = \frac{1}{2}C\dot{\phi}^2 + \frac{1}{2L}\phi^2 = \frac{Q^2}{2(C + C_g)} + \frac{1}{2L}\phi^2. \tag{3.26}$$

If we turn on V_g and disregard terms that do not involve dynamical variables, we obtain

$$H = H_{LC} + \frac{C_g}{C + C_g}V_g Q. \tag{3.27}$$

We can now, similarly to the momentum operator in the harmonic oscillator, re-express Q in terms of the raising and lowering operators of a single excitation of the resonator,

$$Q = -iQ_{zpf}(a - a^\dagger), \tag{3.28}$$

where $Q_{zpf} = \sqrt{\frac{\hbar}{2Z}}$ is the zero-point fluctuation of the charge variable, with Z the impedance of the circuit. Fluctuations arise due to the wave functions having non-zero standard deviations, partly due to the uncertainty principle, even in the ground-state, where they are called zero-point fluctuations [17].
H_{LC} is equivalent to the one dimensional quantum harmonic oscillator with the capacitance C replacing the mass m and resonant frequency $\omega_{01} = 1/\sqrt{LC}$, so can also be recast using the ladder operators,

$$H_{LC} = H_{QHO} = \hbar\omega_{01}(a^\dagger a + 1/2). \tag{3.29}$$

In total we attain

$$H = \hbar\omega_{01}(a^\dagger a + 1/2) - iQ_{zpf}\frac{C_g}{C + C_g}V_g(a - a^\dagger). \tag{3.30}$$

If we only consider the lowest transition of the obtained oscillator, we can exchange a and $a^\dagger$ for σ^- and σ^+

$$H = \hbar\frac{\omega_{01}}{2}\mathbb{1} - \hbar\frac{\omega_{01}}{2}\sigma_z + \Omega V_g\sigma_y, \tag{3.31}$$

with $\Omega = Q_{zpf}C_g/(C_g + C)$ and $\omega_{01} = (E_1 - E_0)/\hbar$. Moreover, by omitting the rigid shift, we write the Hamiltonian as the sum of H_0 and the driving term H_d. Driven dynamics are conveniently described in a reference frame which rotates with the qubit's frame at the frequency ω_{01}. The rotation operator is $R = \exp(itH_0/\hbar) = \exp\left(-it\frac{1}{2}\omega_{01}\sigma_z\right)$. From this we can transform the crucial Pauli operators

$$R\sigma_z R^\dagger = \sigma_z, \tag{3.32}$$

$$R\sigma_y R^\dagger = \cos(\omega_{01}t)\sigma_y - \sin(\omega_{01}t)\sigma_x. \tag{3.33}$$

If we only consider the driving part of the Hamiltonian in the rotating frame, we accordingly get

$$H_g = \Omega V_g\left(\cos(\omega_{01}t)\sigma_y - \sin(\omega_{01}t)\sigma_x\right), \tag{3.34}$$

and drive the voltage with a simple oscillatory behaviour with frequency ω_g

$$V_g = V_0 s(t)\sin(\omega_g t + \phi) = V_0 s(t)\left[\cos(\phi)\sin(\omega_g t) - \sin(\phi)\cos(\omega_g t)\right], \tag{3.35}$$

where ϕ now is the set phase of the drive. Combining both, we end up with

$$H_g = \Omega V_0 s(t)\left[\cos(\phi)\sin(\omega_g t) - \sin(\phi)\cos(\omega_g t)\right]\left[\cos(\omega_{01}t)\sigma_y - \sin(\omega_{01}t)\sigma_x\right], \tag{3.36}$$

for the driving Hamiltonian. We now perform the rotating wave approximation, in which fast oscillating terms are dropped, i.e. terms at frequencies $\omega_g + \omega_{01}$. In the subsequent analysis we also assume that the drive has no detuning, meaning that

we drive the AC power source at the qubit frequency, $\omega_g = \omega_{01}$. Let us expand the drive Hamiltonian, eq. 3.36, and see what terms survive after the RWA

$$\begin{aligned} H_g &= \Omega V_0 s(t)\big[\cos(\phi)\sin(\omega_{01}t)\cos(\omega_{01}t)\sigma_y - \cos(\phi)\sin(\omega_{01}t)\sin(\omega_{01}t)\sigma_x + \\ &\qquad - \sin(\phi)\cos(\omega_{01}t)\cos(\omega_{01}t)\sigma_y + \sin(\phi)\cos(\omega_{01}t)\sin(\omega_{01}t)\sigma_x\big] \\ &= \frac{\Omega V_0 s(t)}{2}\big[\cos(\phi)\cancel{\sin(2\omega_{01}t)}\sigma_y - \cos(\phi)(1 - \cancel{\cos(2\omega_{01}t)})\sigma_x + \\ &\qquad - \sin(\phi)(1 + \cancel{\cos(2\omega_{01}t)})\sigma_y + \sin(\phi)\cancel{\sin(2\omega_{01}t)}\sigma_x\big] \\ &= \frac{\Omega V_0 s(t)}{2}\big(-\cos(\phi)\sigma_x - \sin(\phi)\sigma_y\big). \end{aligned}$$

With all these assumptions, we finally end up with the driving Hamiltonian for the Cooper pair box, where we dropped the subscript g,

$$H(\theta, \phi) = \frac{\theta\hbar}{2} R_{xy}(\phi), \tag{3.37}$$

with $R_{xy}(\phi) = \cos(\phi)\sigma_x + \sin(\phi)\sigma_y$. For simplicity, in this work we consider constant pulses, i.e. $s(t) = s$ and thus define $\theta = -\Omega V_0 s/\hbar$.
The implemented unitaries are therefore of the form

$$U(\theta, \phi) = \exp\left(-\frac{i}{\hbar}H(\theta, \phi)\right) = \exp\left(-\frac{i\theta}{2}R_{xy}(\phi)\right), \tag{3.38}$$

driven for a time interval $t = 1$ and can be applied as a sequence of gates of the form [15]

$$U_K ... U_1 U_0 = \mathcal{T}\left[\prod_{n=0}^{K} \exp\left(-\frac{i\theta_n}{2}R_{xy}(\phi_n)\right)\right], \tag{3.39}$$

where $\mathcal{T}$ is the time-ordering operator, in order to ensure that the pulses are performed in ascending order.
Let us look into more detail, which explicit gates we can achieve with this type of unitary. More importantly, if we can show that for a single-qubit, all Bloch rotations are possible. For this, we show that we can implement the X, Y, Z-gates and the Hadamard gate [15].

For different combinations we can achieve, apart from a constant phase shift,

$$U(\pi, 0) = -i\sigma_x = \sigma_z\sigma_y, \tag{3.40}$$

$$U(\pi/2, 0) = i\sigma_y = \sigma_z\sigma_x, \tag{3.41}$$

from which we can acquire the σ_z gate, since $\sigma_x\sigma_y = i\sigma_z$. Note, we can see the introduced phase shift as changing rotations around x to rotations around y and vice versa, and therefore can be interpreted as effectively applying virtual Z-gates. The Hadamard gate can be achieved by $H = \sigma_x\sigma_y^{(1/2)}$, so a $\pi/2$ rotation around the y-axis followed by a π rotation around the x-axis. Explicitly,

$$U(\pi, 0)U(\pi/2, \pi/2) = -i\sigma_x \left[\frac{1}{\sqrt{2}}\mathbb{1} - i\frac{1}{\sqrt{2}}\sigma_y\right] = -i\frac{1}{\sqrt{2}}\left[\sigma_x + \sigma_z\right] = -iH. \tag{3.42}$$

3.3 Two-qubit gate

Building on the use of the capacitive coupling to a microwave resonator, one can extend the previous approach to the implementation of two qubit gates. The cross-resonance (CR) gate applies to two fixed frequency transmons coupled through a resonator [18] and has recently been utilized to achieve a CNOT gate with high fidelity exceeding 0.99 [19]. We report here the final effective Hamiltonian whose derivation can be found in [20].

$$H^{1,2}(\theta, \phi) = \frac{\theta\hbar}{2} Z \otimes R_{xy}(\theta, \phi), \tag{3.43}$$

which implements unitaries of the form

$$U^{1,2}(\theta, \phi) = \exp\left(-\frac{i\theta}{2} Z \otimes R_{xy}(\theta, \phi)\right), \tag{3.44}$$

again for a duration of $t = 1$.

3.4 Noise

One contributions to decoherence of the system stems from depolarization [21], which, as mentioned before, can be thought of as causing random rotations in the Bloch sphere representation of the qubit. The result is that the quantum state evolves into the completely mixed state at the origin of the Bloch sphere. The other mechanisms present are damping in the z-axis (longitudinal noise, along the quantization axis) and in the $x - y$ plane (transverse noise). They are mainly induced by interactions with the surrounding environment and occur due to thermalization towards equilibrium and result in a damping of both the excited state as well as the coherences of the qubit. The energy exchange between the qubit and its environment generates the longitudinal relaxation to the ground state $|0\rangle$ with rate T_1. Note, in theory we also have induced transitions from ground to excited state by couplings to black body radiation, but the way transmon qubits are normally operated, the frequency of the qubit is much higher than the thermal energy of the operating temperature, they are greatly suppressed. The decoherence effect that contribute to the transverse relaxation (T_2) combines both energy relaxation and pure dephasing in the transverse plane, which originates from fluctuations in the qubit frequency. If the qubit frequency is not equal to the rotating frame frequency, the Bloch vector will effectively precess around the z-axis in the rotating frame eventually causing the $x - y$ plane to be depolarized. The decay functions of the relaxations considered so far are exponential. In superconducting qubits, however, the dephasing noise (e.g. charge noise) is broadband and typically exhibits a 1/f-like power spectrum. Such noise is singular at $\omega = 0$, has long correlation times, and generally the description adopted so far does not apply. For this reason, the decay function of the off-diagonal terms in the qubit density matrix becomes in general non-exponential.
Let us continue, by writing the relevant Lindblad terms for the different noise mechanisms. As discussed in section 1.5, the Lindblad term for depolarization is expressed by

$$\mathcal{D}_d(\rho) = \gamma_d \sum_{k=1}^{3} [\sigma_k \rho \sigma_k - \rho] \tag{3.45}$$

with $\sigma_1 = X$ etc. and $\gamma_d \geq 0$ gives the rate at which depolarization occurs.
Amplitude damping can be expressed by [6]

$$\mathcal{D}_a(\rho) = \gamma_1 \left[\sigma_+ \rho \sigma_- - \frac{1}{2} \left\{ \mathcal{P}_{(1)}, \rho \right\} \right], \tag{3.46}$$

where $\sigma_\pm = (\sigma_x \pm i\sigma_y)/2$ are the Pauli jump operators, $\mathcal{P}_{(1)} = |1\rangle\langle 1|$ and γ_1 gives the rate at which amplitude relaxation occurs.
Note, this expression is equal to the previously defined channel for amplitude damping, as can be seen by explicitly expanding the matrices

$$\begin{aligned} \mathcal{D}_a(\rho) =& \gamma_1 \Bigg\{ \begin{bmatrix} 0 & 1 \\ 0 & 0 \end{bmatrix} \begin{bmatrix} \rho_{00} & \rho_{01} \\ \rho_{10} & \rho_{11} \end{bmatrix} \begin{bmatrix} 0 & 0 \\ 1 & 0 \end{bmatrix} - \frac{1}{2} \begin{bmatrix} 0 & 0 \\ 0 & 1 \end{bmatrix} \begin{bmatrix} \rho_{00} & \rho_{01} \\ \rho_{10} & \rho_{11} \end{bmatrix} & (3.47) \\ & - \frac{1}{2} \begin{bmatrix} \rho_{00} & \rho_{01} \\ \rho_{10} & \rho_{11} \end{bmatrix} \begin{bmatrix} 0 & 0 \\ 0 & 1 \end{bmatrix} \Bigg\} & (3.48) \\ =& \gamma_1 \begin{bmatrix} \rho_{11} & -\frac{\rho_{01}}{2} \\ -\frac{\rho_{10}}{2} & -\rho_{11} \end{bmatrix}. & (3.49) \end{aligned}$$

Furthermore, the Lindblad term for pure dephasing is as before

$$\mathcal{D}_p(\rho) = \gamma_z \left[Z\rho Z - \rho \right], \tag{3.50}$$

where $\gamma_z = (2T_1 - T_2)/(4T_1T_2)$. In this case, we have a dephasing term that enters from relaxation of the excited state (T_1) and a term coming from pure dephasing (T_2), which have to be taken into account [7].
The total Lindblad term is then

$$\mathcal{D}(\rho) = \mathcal{D}_d(\rho) + \mathcal{D}_a(\rho) + \mathcal{D}_p(\rho), \tag{3.51}$$

which we write in the general Lindblad form,

$$\mathcal{D}(\rho) = \epsilon^2 \sum_{k=1}^{3} \left[L_k \rho L_k^\dagger - \frac{1}{2} \left\{ L_k^\dagger L_k, \rho \right\} \right]. \tag{3.52}$$

There are other noise terms that we have not included yet, that can be added similarly into the algorithm. They include correlated errors (in the case of more

qubits) and state preparation and measurement errors that occur before and after the execution of the gate, which are represented by bit-flip channels.

3.5 Results

In this section, we show results for implementing sequences of X-gates on single-qubit and sequences of CR-gates on two-qubit systems. The system dynamics can be worked out to include noise terms in the form of a Linbladian

$$\frac{d\rho_s}{ds} = -\frac{i}{\hbar}\left[H_s, \rho_s\right] + \mathcal{D}(\rho_s), \tag{3.53}$$

where the evolution is driven for $s \in [0, 1]$ with $s = t/t_g$ (t_g the duration of a gate). As discussed, we implement the noiseless Hamiltonian H_s and the noise terms $\mathcal{D}(\rho_s)$ into the noisy gate formalism. We move from the density matrix formalism to the state vector formalism, by performing a linear stochastic unraveling of the Lindbald equation. As discussed in Chapter 1, this approach requires the solution of

$$\Lambda = -\frac{\epsilon^2}{2}\int_0^1 ds \sum_{k=1}^{N^2-1}[L_{k,s}^\dagger L_{k,s} - L_{k,s}^2], \tag{3.54}$$

$$\Xi = i\epsilon \sum_{k=1}^{N^2-1}\int_0^1 dW_{k,s} L_{k,s}. \tag{3.55}$$

Finally, this procedure allows the definition of noisy gates of the form

$$N_g = U_g e^{\Lambda} e^{\Xi}. \tag{3.56}$$

In Appendix A.2, we show for the single-qubit case exactly how to calculate the Lindblad operators in the interaction picture and how to sample the obtained Wiener integrals. To obtain our results, we build a Python class that modifies a given unitary Hamiltonian with the appropriate noisy terms. We then use the modified matrices to implement an evolution of an initial state vector, by repetitively applying the noisy gate. The algorithm is sketched below for the case of superconducting single-qubit gates.

Algorithm 1 Noisy gate for superconducting single qubit

Function *scqSingleQubitSampleRun(psi0, N, shots)*

Input : ψ_0 is the initial state vector

Input : N the number of gates to be applied

Input : *shots* the number of samples to take the average of

0.1 Initialize noiseless circuit $C = [U_g \text{ for } j \text{ in range}(N)]$

0.2 Calculate deterministic part of noisy gate Λ

0.3 **for** *i in shots* **do**

0.4 **for** $1 \leq k \leq N$ **do**

0.5 Sample stochastic process and calculate stochastic part Ξ

0.6 Compute $|\psi_k\rangle = U_g e^{\Lambda} e^{\Xi} |\psi_{k-1}\rangle$

0.7 Compute $\rho_k = |\psi_k\rangle \langle\psi_k|$

0.8 Save ρ_k into results array

0.9 Calculate for each k in results: $\rho_k = \rho_k / shots$

0.10 **return** results

For the simulation we use the qubit noise parameters of the ibmq Manila device [22, 23]. The Manila device has 5 fixed-frequency transmon qubits and thus can be used as a reference for our single-qubit, as well as two-qubit simulations. At the point of determination, in two-qubit mode, the parameters read $T_{1,ctr} = 138.98\,\mu s$ and $T_{2,ctr} = 112.21\,\mu s$ for the control qubit and $T_{1,trg} = 152.35\,\mu s$ and $T_{2,trg} = 83.655\mu s$ for the target qubit. Furthermore, the depolarization characteristic time was given as $T_d = 321.62\,\mu s$. For the single-qubit simulation, we used the parameters for the control qubit $T_{1,ctr}$ and $T_{2,ctr}$. Lastly, for all simulations, we used a gate time of $t_g = 35$ ns.

In the following, we present three examples: First, we use a noisy identity Hamiltonian and an X-gate on a single-qubit and then, we apply a CR-gate sequence on a two-qubit system.

In the first example, we initialize the qubit in the state $|1\rangle$ and apply a repetition of noisy identity Hamiltonians. This effectively simulates preparing a qubit in a definite state and observing its evolution over a specified period in the presence of considered noise. The behaviour can be seen in figure 3.3.

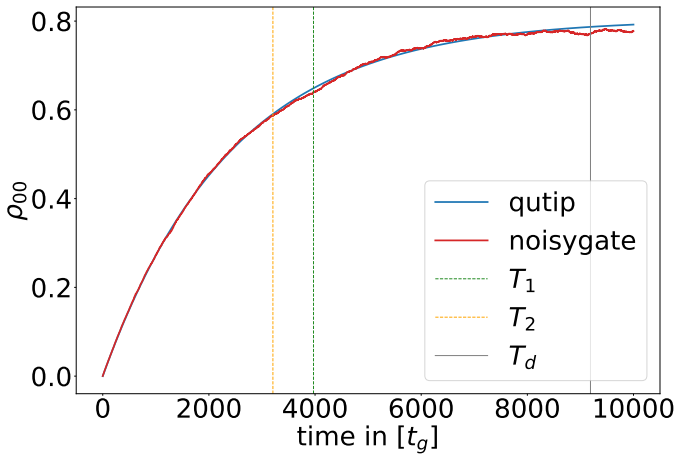

Figure 3.3: The time-evolution of the ρ_{00} entry is shown for a repetition of identity gates on a qubit initially in the $|1\rangle$ state. We display both qutip (blue) and noisy gates algorithm (red), where the average is taken over 5000 samples. $T_1 = 138.98$ µs, $T_2 = 112.21$ µs and $T_d = 321.62$ µs represent the relaxation times for the considered damping processes and the values refer to the IBM Manila device.

As anticipated, the $|0\rangle$ state increasingly gets populated due to the presence of amplitude damping. In Figure 3.3, we also highlight the characteristic times of the different noise channels, T_1,T_2 and T_d. Both simulations asymptotically converge to a seemingly arbitrary value. The steady state is determined by the competition between depolarization and amplitude damping. The first one drives the system towards the mixed state while the second one towards the ground state. The final value can be straight forwardly found, by calculating the steady state solution of the dissipator, equation 3.51,

$$\mathcal{D}(\rho) \stackrel{!}{=} 0, \tag{3.57}$$

which is readily evaluated, yielding

$$\begin{aligned}
\rho_{00} =& \frac{\gamma_2}{\gamma_1 + \gamma_2}; \\
\rho_{11} =& \frac{\gamma_1}{\gamma_1 + \gamma_2}; \\
\rho_{01} =& \rho_{10} = 0.
\end{aligned}$$

In our specific case, with this solution we predict a steady state $\rho_{00} \sim 0.81$.
We now look at an evolution with a single-qubit noisy gate as derived in equation

3.38. The results can be seen in figure 3.4. We are initializing the state $|1\rangle$ and evolve it, using a repetition of X-gates for a total time of Nt_g, with $N = 10000$. The X-gate is constructed by choosing $\theta = \pi$ and $\phi = 0$ in our single-qubit Hamiltonian.

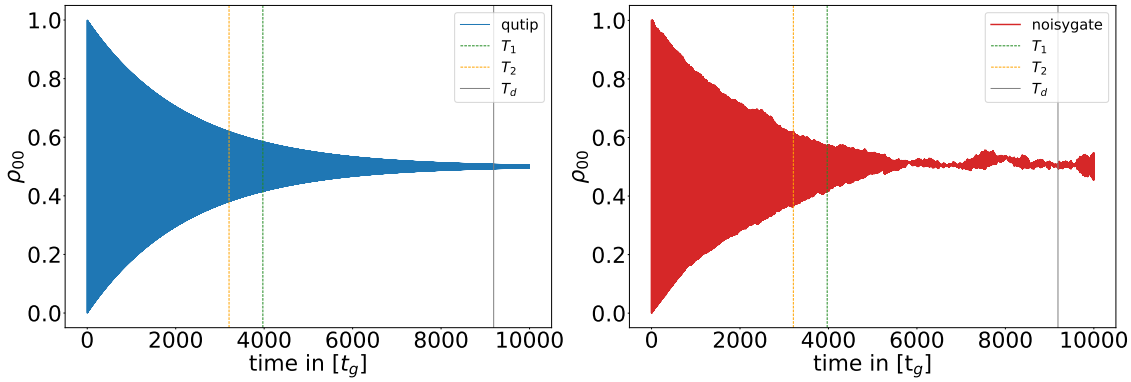

(a) **(b)**

Figure 3.4: Repetition of X-gates on a single qubit initialized in the $|0\rangle$ state. We show the time-evolution of the ρ_{00} term. We compare the evolution computed with qutip (a) to the one obtained with the noisy gate after 1000 samples (b). Again, $T_1 = 138.98\,\mu s$, $T_2 = 112.21\,\mu s$ and $T_d = 321.62\,\mu s$ represent the relaxation times for the considered processes and the values refer to the IBM Manila device.

The values for T_1, T_2, T_d and the gate time t_g are the same as in the previous example. We see oscillations between $|0\rangle$ and $|1\rangle$ as expected from reapplying the X-gate. The oscillations are damped due to the presence of noises and we asymptotically reach the value $\rho_{00} = 0.5$. Contrary to the "rest" evolution before, both depolarization and amplitude damping drive the system towards the totally mixed state ($\rho_{00}, \rho_{11} = 0.5$) because of the repetition of X-gates.
Lastly, we show the implementation of the two-qubit cross resonance (CR) gate. The effect of a repetition of this gate onto a prepared state can be seen in figure 3.5. This time, we evolve for a duration of Nt_g with $N = 10000$. We implement the CR-gate as $\theta = \pi$ and $\phi = 0$. The resulting Hamiltonian is $H^{1,2} = \frac{\pi\hbar}{2} Z \otimes X$. We initialize the qubit in the $|11\rangle$ state and the effect of this Hamiltonian is an oscillation between $|11\rangle$ and $|10\rangle$.

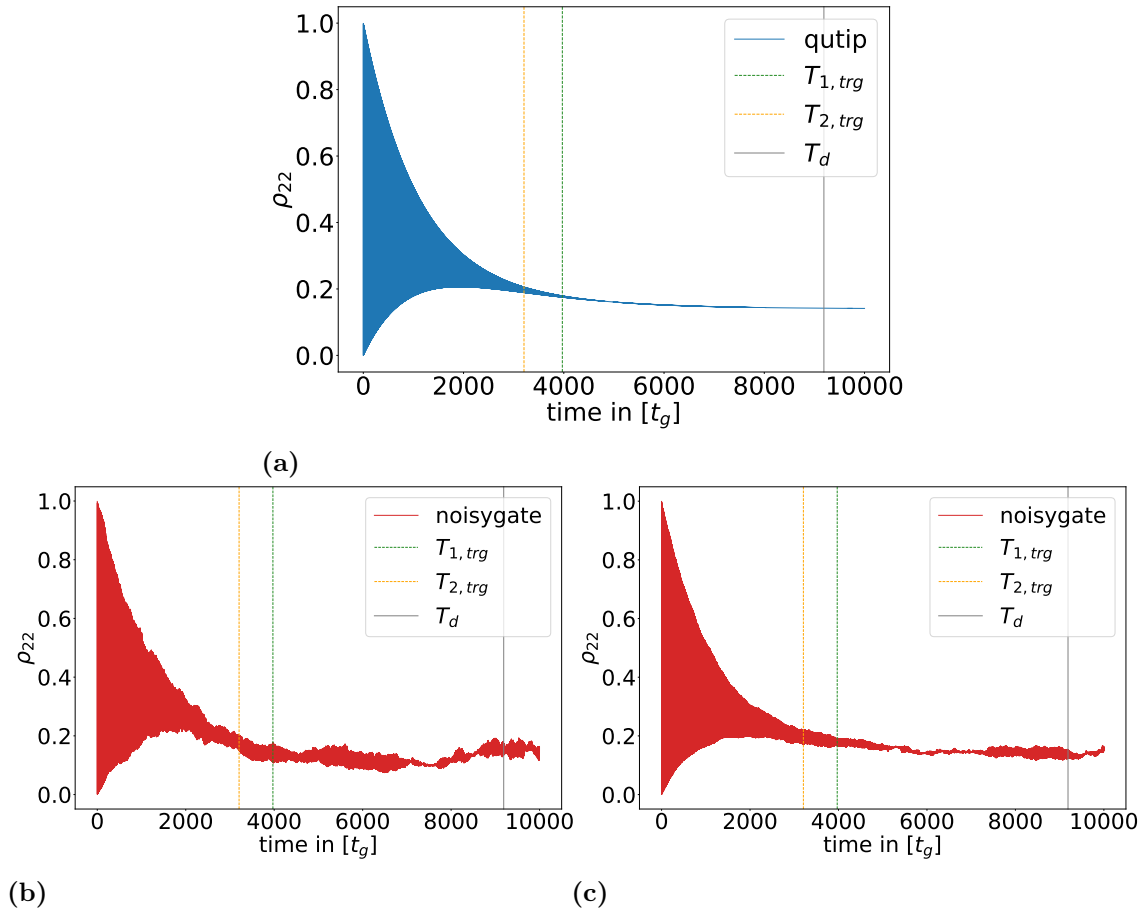

Figure 3.5: Repetition of CR-gates on a two qubit initialized in the $|11\rangle$ state. We show the time-evolution of the ρ_{22} term. The qutip evolution is given in (a). The noisy gate plots are a result of (b) 100 and (c) 1000 samples. The characteristic relaxation times are given by $T_{1,ctr} = 138.98\,\mu s$, $T_{2,ctr} = 112.21\,\mu s$ for the control qubit and $T_{1,trg} = 152.35\,\mu s$, $T_{2,trg} = 83.655\,\mu s$ for the target qubit. Furthermore, the depolarization characteristic time is given by $T_d = 321.62\,\mu s$.

From the examples, we can see that we qualitatively reproduce the behaviour of the exact solution in each evolution. Furthermore, the more samples we take into account, the more accurately we reproduce the exact solution, which makes sense, since we expect to recover the exact solution in the large sampling limit due to the unraveling of the Schrödinger equation done in the preceding steps, meaning we are averaging out the noise.
This means that we have a strong indication that we implemented the algorithm correctly and can use it to simulate novel problems.

4

Rydberg hardware

In this chapter, we first introduce the Rydberg atom, derive the implemented single- and two-qubit unitaries starting from a semi-classical analysis of the interaction between light and matter. After having discussed the relevant noises on this hardware, we extend the noisy gate protocol to this architecture and consider single and two-qubit gates implemented on a rubidium platform.

A prospective approach for quantum computations utilizes arrays of neutral atoms, specifically Rydberg atoms, where individual atoms serve as qubits. The initialization and manipulation of their states are achieved through electromagnetic fields [24]. Optical tweezers, generated by tightly focused laser beams, trap these atoms by exerting an attractive force, which causes atoms to be drawn toward regions of high intensity, namely the focus [25].
Next, individually shaped laser pulses are used to stimulate Rabi oscillations in the atoms, coupling the ground states to specific Rydberg states. These are states in which the valence electron is in a large and loosely bound orbit. Rydberg atoms are particularly interesting because of their large electric dipole momenta, which makes them couple strongly to external electromagnetic radiation and thus easily addressable. Also, as the interaction among Rydberg atoms is very weak when they are more than few angstrom apart, many atoms can be packed close together in a quantum register. However, qubit interactions are essential for implement-

ing entangling gates. One effective solution involves temporarily exciting atoms to Rydberg states. This exploits the Rydberg blockade mechanism, preventing simultaneous excitation of more than one atom to a Rydberg state within a confined volume, thereby facilitating entanglement between two qubits.

4.1 Rydberg atoms

Since Rydberg atoms resemble closely hydrogen atoms, it is instructive to first discuss the solution of the hydrogen atom. It's Hamiltonian is given by [25]

$$H = \left\{ \frac{-\hbar^2}{2m_e} \nabla^2 + V(r) \right\} \psi = E\psi, \tag{4.1}$$

with $V(r)$ the spherically symmetric Coulomb potential and m_e the electronic mass. To solve it, we look for solutions of the form $\psi = R(r)Y(\theta, \phi)$ in spherical coordinates.
With this, the Schrödinger equation becomes

$$\frac{1}{R}\frac{\partial}{\partial r}\left(r^2 \frac{\partial R}{\partial r}\right) - \frac{2m_e r^2}{\hbar^2}\left(V(r) - E\right) = \frac{1}{Y}\mathbf{l}^2 Y, \tag{4.2}$$

where we write the nabla operator in terms of spherical coordinates, with

$$\mathbf{l}^2 = -\left(\frac{1}{\sin\theta}\frac{\partial}{\partial\theta}\left(\sin\theta\frac{\partial}{\partial\theta}\right) + \frac{1}{\sin^2\theta}\frac{\partial^2}{\partial\phi^2}\right). \tag{4.3}$$

Each side depends on different variables, for the equation to be valid we thus need each side to be equal to a constant. We can then turn to solve for the radial R and the angular part Y separately. In fact, the one-electron system is the only atom which can be solved exactly, while for atoms with more electrons we have to turn to approximations.
Figure 4.1 shows some solutions to the radial part of the hydrogen Hamiltonian. The left plot, 4.1a, indicates how the mean radius increases as the principal quantum number n increases, while the wave function becomes more dispersed. The right plot, 4.1b, indicates that as l approaches n, the wave function becomes highly localized again. It can be shown, that the mean radial expectation value follows

$\langle r \rangle = n^2 a_0$, with a_0 the Bohr radius, when $l = n - 1$.
Rydberg atoms are generally atoms with one or more electrons occupying a state with a high principal quantum number, typically $n > 11$. In particular, when the orbital quantum number $l \sim n$, so that the electron is localized and it's orbit nearly circular, they are called circular Rydberg atoms. In this work, we assume to deal with one-valence electron systems, meaning hydrogenic Rydberg atoms for simplicity.

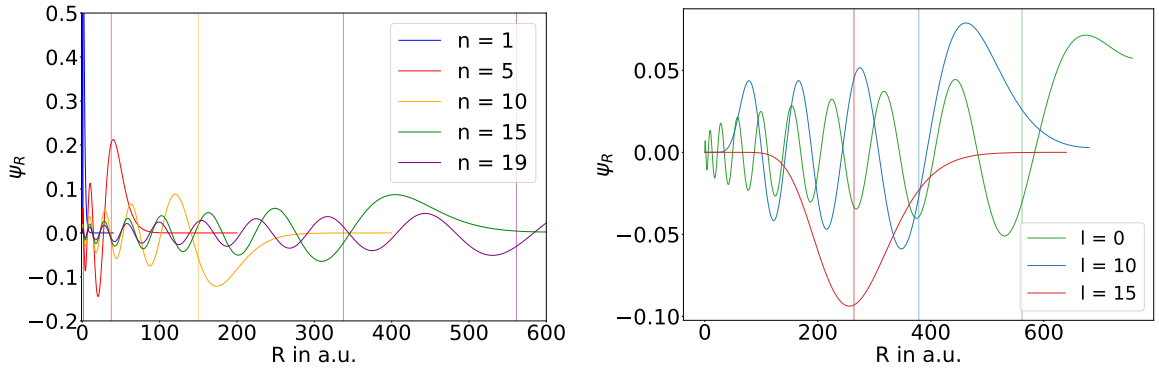

(a) **(b)**

Figure 4.1: Radial wave functions for hydrogen, (a) shows some s-orbitals for increasing principal quantum number n, the vertical lines show the radial expectation value. On the other hand, (b) shows some wave functions for high $n = 19$, varying the orbital quantum number l. The solutions are obtained by solving the radial Schrödinger equation for a Coulomb potential $V(r) = -Z/r$ using Numerov's method under the constraint of reaching $n - l - 1$ number of nodes. The vertical lines show the radial expectation value, calculated as $\langle r \rangle = \Delta r \sum_i r \psi_R^2$, where Δr is the mesh size.

In the hydrogen atom, the binding energy of the electron is given by the Rydberg formula,

$$\frac{1}{\lambda} = -R_H \frac{1}{n^2}, \tag{4.4}$$

where n is the principle quantum number describing the energy level the electron is residing in and $R_H = R_\infty/(1+m_e/M) = 1.097 \cdot 10^7 \mathrm{m}^{-1}$ is the Rydberg constant of the hydrogen atom, where M is the mass of the core. Furthermore, since we consider only one valence electron atoms, we can use the fact that the effective potential the valence electron sees tends to approximate that of a hydrogenic atom for large orbital radii. As the valence electron gets highly excited, the radius of it's

orbit increases with the square of the principle quantum number, thus the overlap of it's orbital and the ionic core becomes negligible. In this case the other electrons effectively shield the protonic core and thus the valence electron sees a hydrogenic potential. However, we have seen that the electron becomes highly dispersed as the orbital quantum number l becomes lower, eventually penetrating the core and thus destroying the approximation. For these cases we can make use of the quantum defect. The formula 4.4 can be extended to include alkaline atoms by introducing the phenomenological concept of the quantum defect: the quantum defect δ_l is subtracted from the principal quantum number and an effective principal quantum number n^* is obtained

$$\frac{1}{\lambda} = -R_H \frac{1}{n^{*}2}, \tag{4.5}$$

with $n^* = n - \delta_{lj}$, which depends on the orbital quantum number and is anticipated to converge towards n for large l.
In general, the lifetime of a Rydberg state is given by

$$\frac{1}{\tau} = \frac{1}{\tau_0} + \frac{1}{\tau_{bb}}, \tag{4.6}$$

with radiative lifetime

$$\frac{1}{\tau_0} = \sum_{n'} A_{nn'}, \tag{4.7}$$

where $A_{nn'}$ are the Einstein coefficients for spontaneous emission from state n to n'. For a low orbital quantum number, the state has a large number of dipole allowed transitions and it's lifetime scales as n^{-3}, while for large l states the number rapidly decreases and the lifetime in turn scales as n^{-5} [24]. In particular, in the limit case, $l = n - 1$ the only possible spontaneous decay channel is the transition to the next lower circular state.
The second main contribution to the lifetime, τ_{bb}, resides in interactions with black body radiation. Rydberg states have very low frequency transitions and thus couple to room-temperature black body radiation. For large n the blackbody

rate is given by [26]

$$\frac{1}{\tau_{bb}} = \frac{4\alpha^3 k_B T}{3\hbar n^{*2}}, \tag{4.8}$$

where α is the fine structure constant, k_B the Boltzmann constant and T the considered temperature.
Now that we have characterized Rydberg atoms and given qualitatively the motivation behind using their exaggerated properties as a means for quantum information, we take a small leap and look in general how light interacts with atoms from a semi-classical point of view.

4.2 Light-matter interaction

If we want to prepare and drive an atomic state, such as a Rydberg state in a Rydberg atom, we use optical fields, thus it is instructional to discuss general light-atom interaction from a semiclassical picture. Semiclassical in the sense that we describe the electromagnetic field as classical, but use quantum mechanics to describe the atom.
We consider an atom exposed to an electric field with frequency ω_L and only consider relevant coupling between two states, also known as the two-level approximation. The monochromatic field can be written as

$$\mathbf{E}(t) = \hat{\mathbf{r}} E_0 \cos(\omega_L t). \tag{4.9}$$

The light source is detuned by an amount $\Delta = \omega_L - \omega_0$, where ω_0 is the transition frequency between the two considered states.
The Hamiltonian that describes the electric dipole interaction is given by

$$\hat{H}_I = -\hat{\mathbf{d}} \cdot \mathbf{E}(t) = -(\hat{\mathbf{r}} \cdot \hat{\mathbf{d}}) \frac{E_0}{2} \left(e^{i\omega_L t} + e^{-i\omega_L t} \right). \tag{4.10}$$

Here, we can define the Rabi frequency $\Omega = (\hat{\mathbf{d}} \cdot \hat{\mathbf{r}}) \frac{E_0}{\hbar}$ and rewrite the expression as

$$\hat{H}_I = \frac{\hbar\Omega}{2} \left(e^{i\omega_L t} + e^{-i\omega_L t} \right) \left(|g\rangle \langle e| + |e\rangle \langle g| \right) \tag{4.11}$$

The Hamiltonian of the atom on the other hand is given by

$$\hat{H}_0 = \hbar\omega_0 \left|e\right\rangle \left\langle e\right|, \tag{4.12}$$

and combining both gives the full Hamiltonian $\hat{H} = \hat{H}_0 + \hat{H}_I$,

$$\hat{H} = \hbar \begin{pmatrix} 0 & \frac{\omega^*}{2}\left(e^{i\omega_L t} + e^{-i\omega_L t}\right) \\ \frac{\omega}{2}\left(e^{i\omega_L t} + e^{-i\omega_L t}\right) & \omega_0. \end{pmatrix}. \tag{4.13}$$

The wavefunction at any given time can be written as

$$\left|\psi\right\rangle = c_1(t)\left|g\right\rangle + c_2(t)\left|e\right\rangle, \tag{4.14}$$

substituting into the time-dependent Schrödinger equation yields

$$i\dot{c}_1 = \frac{\Omega^*}{2}\left(e^{i\omega_L t} + e^{-i\omega_L t}\right) c_2 \tag{4.15}$$

$$i\dot{c}_2 = \frac{\Omega}{2}\left(e^{i\omega_L t} + e^{-i\omega_L t}\right) c_1 + \omega_0 c_2. \tag{4.16}$$

We can make a substitution in order to swap to the rotating frame by $\tilde{c}_1 = c_1$ and $\tilde{c}_2 = c_2 e^{i\omega_L t}$

$$i\frac{\partial \tilde{c}_1}{\partial t} = \frac{\Omega^*}{2}\left(1 + e^{-i2\omega_L t}\right)\tilde{c}_2 \tag{4.17}$$

$$i\frac{\partial \tilde{c}_2}{\partial t} = \frac{\Omega}{2}\left(1 + e^{-2i\omega_L t}\right)\tilde{c}_1 - \Delta\tilde{c}_2. \tag{4.18}$$

Within the rotating wave approximation we can neglect the terms oscillating at $2\omega_L$ and thus we get

$$i\frac{\partial \tilde{c}_1}{\partial t} = \frac{\Omega^*}{2}\tilde{c}_2 \tag{4.19}$$

$$i\frac{\partial \tilde{c}_2}{\partial t} = \frac{\Omega}{2}\tilde{c}_1 - \Delta\tilde{c}_2, \tag{4.20}$$

and corresponding Hamiltonian

$$H_{rwa} = \hbar \begin{pmatrix} 0 & \frac{\Omega^*}{2} \\ \frac{\Omega}{2} & -\Delta \end{pmatrix}. \tag{4.21}$$

The solution to this Hamiltonian are characteristic Rabi oscillations: the electromagnetic field continuously drives transitions between the two considered states. We plot some of them for different combinations of detuning Δ and Rabi frequency Ω in figure 4.2. We stress that introducing large detuning into the dynamics effectively damps the oscillations, a result that will play an important role in the two-atom dynamics of Rydberg atoms.

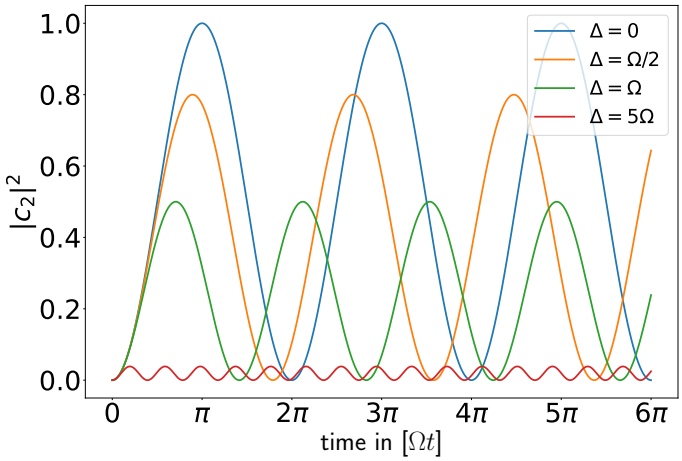

Figure 4.2: The probability for the two-level atom to be in the excited state with respect to elapsed time. We plot different combinations of detuning Δ and Rabi frequency Ω, which show that the introduction of detuning leads to the oscillations having higher frequency, but get increasingly damped for $\Delta > \Omega$.

4.3 Rydberg-Rydberg interaction

In order to produce entanglement with Rydberg atoms, we need to consider more than one atom and discuss how different Rydberg atoms interact with each other. Since Rydberg atoms posses large dipole moments, the main contribution in the multipolar expansion of the electric potential comes from dipole-dipole interactions between adjacent atoms. The corresponding potential term is given by [24]

$$V_{dd} = \frac{e^2}{4\pi\epsilon_0} \frac{\mathbf{d}_1 \cdot \mathbf{d}_2 - 3\,(\mathbf{d}_1 \cdot \mathbf{e}_R)\,(\mathbf{d}_2 \cdot \mathbf{e}_R)}{R^3}, \tag{4.22}$$

with dipole moments $\mathbf{d}_i = -e\mathbf{R}_i$, $\mathbf{e}_R$ the unit vector along $\mathbf{R}$ and R the interatomic distance. From before we can work out the n dependence, since $\mathbf{d}$ scales as n^2, V_{dd} will scale as n^4.

Let us model the interaction for a two atom system, with each atom having one electron in a Rydberg state. With no external electric field, the atoms are unpolarized and thus have a vanishing dipole moment. In that case the dipole interaction operator acts as a second order perturbation, by coupling the two Rydberg states to other pair states of opposite parity [27, 28], which results in a interaction energy of the form [29]

$$C_{rr} = \sum_{|cd\rangle} \frac{\langle rr| V_{dd} |cd\rangle \langle cd| V_{dd} |rr\rangle}{2E_r - Ec - E_d} = \frac{C_{6,r-r}}{R^6}. \tag{4.23}$$

This corresponds to a Van-der-Waals interaction, where $|cd\rangle$ are all possible intermediate pair states, E_i the energy of the single atom i and $C_{6,r-r}$ the Van-der-Waals coefficient, which can be shown to scale as n^{11} [27].
In order to see the dynamics of a two-atom system, consider for simplicity two atoms that both couple resonantly $|g\rangle$ to $|r\rangle$, i.e.

$$H = \frac{\Omega}{2} \left(|g\rangle \langle r| \otimes \mathbb{1} + \mathbb{1} \otimes |g\rangle \langle r| + H.C. \right) - \frac{C_{6,r-r}}{R^6} |rr\rangle \langle rr| , \tag{4.24}$$

$$= \frac{\Omega}{2} \left(|gg\rangle \langle gr| + \langle gg| rg\rangle + |gr\rangle \langle rr| + |rg\rangle \langle rr| + H.C. \right) - \frac{C_{6,r-r}}{R^6} |rr\rangle \langle rr| . \tag{4.25}$$

Now, we notice that $|\psi_-\rangle = (|gr\rangle - |rg\rangle)/\sqrt{2}$ is an eigenstate of the Hamiltonian with eigenvalue zero. Therefore, we can effectively delete it from the dynamics. This enables us to change the description to an effective three level system with basis states $|gg\rangle$, $|\psi_+\rangle = (|gr\rangle + |rg\rangle)/\sqrt{2}$ and $|rr\rangle$ and get a new expression for the Hamiltonian,

$$H = \frac{\sqrt{2}\Omega}{2} \left(|gg\rangle \langle +| + |+\rangle \langle rr| + H.C. \right) - \frac{C_{6,r-r}}{R^6} |rr\rangle \langle rr| . \tag{4.26}$$

We note the enhancement of the Rabi frequency by a factor of $\sqrt{2}$. Moreover, we identify two interaction regimes that implement different dynamics, determined by the competition between the Rabi frequency Ω and the Van-der-Waals interaction term $C_{6,r-r}/R^6$: When $|C_{6,r-r}|/R^6 \ll \Omega$, the two atoms only weakly interact and we have slightly perturbed Rabi oscillations of the single atoms. In the other regime on the other hand, when $|C_{6,r-r}|/R^6 \gg \Omega$, we introduce strong detuning

in the transition of $|\psi_+\rangle$ and $|rr\rangle$, effectively eliminating $|rr\rangle$ from the dynamics. Then, we can reduce the description even further and express the dynamics as a two-level system, with Hamiltonian

$$H = \frac{\sqrt{2}\Omega}{2}(|gg\rangle\langle\psi_+| + H.C.). \tag{4.27}$$

This regime is referred to as the Rydberg blockade regime, as can be seen in figure 4.3. We see that in this regime, we produce Rabi oscillations with the frequency enhanced by $\sqrt{2}$ between ground and the intermediate $|\psi_+\rangle$ state and that therefore the maximum probability to find an atom in the excited Rydberg state is $1/2$. Usually, the distance at which the two regimes transition is set to be when they are equal, so at the radius when $\Omega = C_{6,r-r}/R_b^6$.

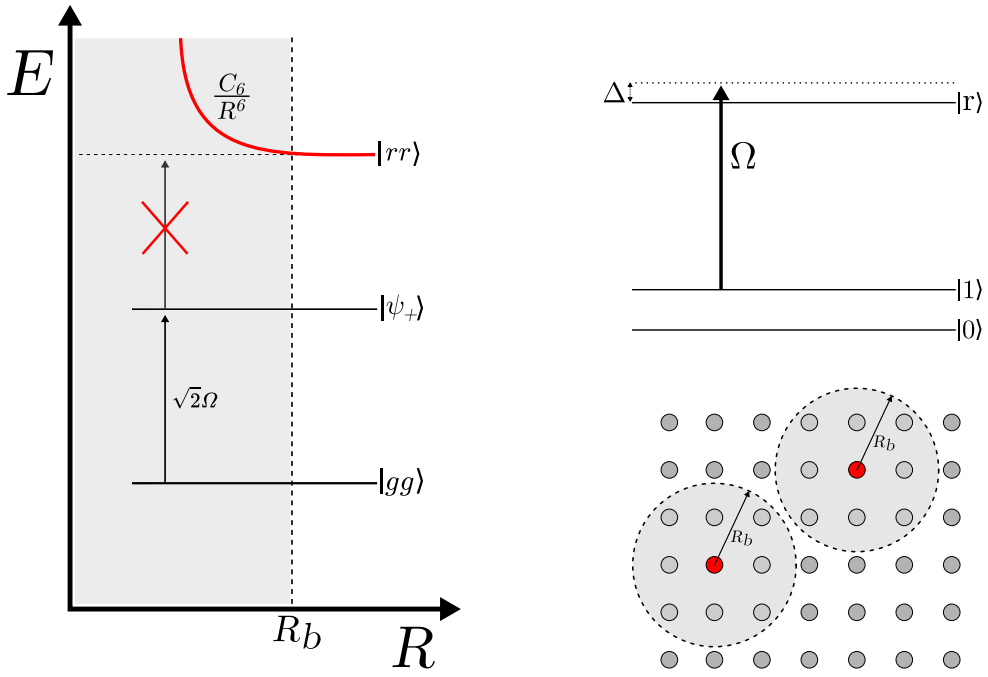

Figure 4.3: Depiction of the Rydberg blockade scheme. In (a) we show the effect of the Van-der-Waals interaction among two Rydberg atoms: In the regime of strong interaction, the transition to the $|rr\rangle$ state is strongly suppressed and we achieve an effective oscillation between $|gg\rangle$ and $|\psi_+\rangle$. If the interatomic distance is above R_b, the interaction is weak and we achieve slightly detuned Rabi oscillations of the single atoms, as can be seen in the top of (b). The bottom of (b) shows how this concept looks qualitatively for a 2d array of neutral atoms: If one atom is excited in the Rydberg state, the interaction prevents atoms within the Rydberg blockade radius to be excited into the same state. Note, here $C_6 = C_{6,r-r}$ from the text.

In the next chapter, we discuss how these single-atom and multi-atom Hamiltonians are used to implement gates on the Rydberg platform and thereby also explain which types of noises are relevant and modify the dynamics.

4.4 Results

We consider a setup, where Rydberg atoms have the quantum information encoded in two low lying hyperfine levels, $|0\rangle$ and $|1\rangle$. To drive single-qubit gates, $|0\rangle$ and $|1\rangle$ are coupled using microwave fields [30]. Two-qubit gates, on the other hand, are driven by coupling the state with higher energy, $|1\rangle$, to the $|r\rangle$ Rydberg state in both atoms, using optical fields [31]. Experimental implementation can be realized using e.g. strontium-88 atoms [5], rubidium-87 [32] or rubidium-85 [33].
Since we generally have dissipation into states that are outside of our computational basis, we introduce another state into our description that we simply call dark state $|d\rangle$, which we use to represent all relaxation channels to states outside our basis. Then our state vector takes the form $|q\rangle = (0, 1, r, d)^T$.
For our simulations, we focus on rubidium, where Rydberg states can reach lifetimes of 50 µs [33]. Similar values also hold for e.g. strontium [5]. Furthermore, the lifetimes of both $|0\rangle$ and $|1\rangle$ are assumed to be $T_a = 4$ s [34].
Generally, evolutions are driven with Rabi frequencies on the order of khZ in single-qubit operations [35, 36, 37] resulting in gate times in the order of µs, while they are driven in the MhZ regime for two-qubit operations [5], resulting in gate times 2-3 orders of magnitude smaller.
The two contributions to considerable decoherence stem from spontaneous decay of both $|0\rangle$ and $|1\rangle$ to states outside of the considered computational basis and dephasing. Contributions to dephasing can result from a variety of sources including, for example, limitations caused by the laser source. These include intensity fluctuations and finite linewidth. They introduce a time-dependent variation in the Rabi frequency, which in turns introduces a phase that leads to dephasing between the two quantum states without causing transitions between them. Other mechanisms that can possibly introduce dephasing can include heating mechanisms within the trap. However, these are more present in multi-atom traps [38]. For the single-qubit operation, we consider a dephasing characteristic time of $T_{dp} = 300$ ms [34].

In the following sections, we define the specific noisy gates for this architecture.

4.4.1 Single-body gate

The Hamiltonian is given within the RWA as

$$H_{rwa} = \hbar \begin{pmatrix} 0 & \frac{\Omega}{2}\xi_1 \\ \frac{\Omega}{2}\xi_2 & -\Delta \end{pmatrix}, \tag{4.28}$$

where we made a slight modification of the Hamiltonian from eq. 4.21 to 4.28 by introducing $\xi_1 = e^{i\mathbf{k}\cdot\mathbf{r}}$ and $\xi_2 = e^{-i\mathbf{k}\cdot\mathbf{r}}$. This parameter should cover an introduced phase shift that arises from misalignment between the atom and the focus of the electromagnetic field $\mathbf{kr}$.
In order to find the time-evolution operator, we diagonalize the Hamiltonian and use the property of the matrix exponential

$$e^A = ue^{\Lambda}u^t, \tag{4.29}$$

whenever $A = u\Lambda u^{-1}$ is a diagonalizeable matrix.
So in order to evaluate

$$U = e^{-\frac{i}{\hbar}Ht}, \tag{4.30}$$

we begin by diagonalizing the argument $-\frac{i}{\hbar}H_{rwa}t$, which yields the eigenvalues

$$\lambda_{1,2} = t\frac{i}{2}\left(\Delta \pm \Omega^{'}\right), \tag{4.31}$$

and the corresponding eigenvectors

$$\phi_{1,2} = \left(-\frac{-\Delta \mp \Omega^{'}}{\Omega\xi_2}, 1\right), \tag{4.32}$$

where we define a generalized Rabi frequency $\Omega^{'} = \sqrt{\Delta^2 + \Omega^2 \xi_1 \xi_2}$.
Having all the ingredients we calculate

$$U = e^{-t\frac{i}{\hbar}H_{rwa}} = \begin{pmatrix} \frac{\Delta+\Omega^{'}}{\Omega\xi_2} & \frac{\Delta-\Omega^{'}}{\Omega\xi_2} \\ 1 & 1 \end{pmatrix} \begin{pmatrix} e^{i/2(\Delta-\Omega^{'})t} & 0 \\ 0 & e^{i/2(\Delta+\Omega^{'})t} \end{pmatrix} \begin{pmatrix} \frac{\Delta+\Omega^{'}}{\Omega\xi_2} & \frac{\Delta-\Omega^{'}}{\Omega\xi_2} \\ 1 & 1 \end{pmatrix}^{-1}, \tag{4.33}$$

where the inverse is readily calculated as

$$\begin{pmatrix} \frac{\Delta+\Omega^{'}}{\Omega\xi_2} & \frac{\Delta-\Omega^{'}}{\Omega\xi_2} \\ 1 & 1 \end{pmatrix}^{-1} = \frac{1}{\frac{2\Omega^{'}}{\Omega\xi_2}} \begin{pmatrix} 1 & \frac{\Omega^{'}-\Delta}{\Omega\xi_2} \\ -1 & \frac{\Delta+\Omega^{'}}{\Omega\xi_2} \end{pmatrix} = \begin{pmatrix} \frac{\Omega\xi_2}{2\Omega^{'}} & \frac{\Omega^{'}-\Delta}{2\Omega^{'}} \\ -\frac{\Omega\xi_2}{2\Omega^{'}} & \frac{\Omega^{'}+\Delta}{2\Omega^{'}} \end{pmatrix}. \tag{4.34}$$

Full evaluation of the matrix then gives

$$\begin{aligned} U &= \begin{pmatrix} \frac{\Delta+\Omega^{'}}{\Omega\xi_2} & \frac{\Delta-\Omega^{'}}{\Omega\xi_2} \\ 1 & 1 \end{pmatrix} \begin{pmatrix} e^{i/2(\Delta+\Omega^{'})t} & 0 \\ 0 & e^{i/2(\Delta-\Omega^{'})t} \end{pmatrix} \begin{pmatrix} \frac{\Omega\xi_2}{2\Omega^{'}} & \frac{\Omega^{'}-\Delta}{2\Omega^{'}} \\ -\frac{\Omega\xi_2}{2\Omega^{'}} & \frac{\Omega^{'}+\Delta}{2\Omega^{'}} \end{pmatrix} \\ &= \begin{pmatrix} \frac{\Delta+\Omega^{'}}{\Omega\xi_2} e^{i/2(\Delta+\Omega^{'})t} & \frac{\Delta-\Omega^{'}}{\Omega\xi_2} e^{i/2(\Delta-\Omega^{'})t} \\ e^{i/2(\Delta+\Omega^{'})t} & e^{i/2(\Delta-\Omega^{'})t} \end{pmatrix} \begin{pmatrix} \frac{\Omega\xi_2}{2\Omega^{'}} & \frac{\Omega^{'}-\Delta}{2\Omega^{'}} \\ -\frac{\Omega\xi_2}{2\Omega^{'}} & \frac{\Omega^{'}+\Delta}{2\Omega^{'}} \end{pmatrix} \\ &= e^{i/2\Delta t} \begin{pmatrix} \cos\left(\Omega^{'}/2t\right) - i\frac{\Delta}{\Omega^{'}} \sin\left(\Omega^{'}/2t\right) & -i\frac{\Omega\xi_1}{\Omega^{'}} \sin\left(\Omega^{'}/2t\right) \\ -i\frac{\Omega\xi_2}{\Omega^{'}} \sin\left(\Omega^{'}/2t\right) & \cos\left(\Omega^{'}/2t\right) + i\frac{\Delta}{\Omega^{'}} \sin\left(\Omega^{'}/2t\right) \end{pmatrix} \end{aligned} \tag{4.35}$$

We can show that this unitary implements all the relevant operations, i.e. for a single-qubit all Bloch rotations are possibly achieved, by finding the combinations of variables that produce the rotation gates [10]:

$$R_x = U(\Delta = 0, \xi_1 = 1, \xi_2 = 1) = \begin{pmatrix} \cos\left(\frac{\Omega t}{2}\right) & -i\sin\left(\frac{\Omega t}{2}\right) \\ -i\sin\left(\frac{\Omega t}{2}\right) & \cos\left(\frac{\Omega t}{2}\right) \end{pmatrix}, \tag{4.36}$$

$$R_y = U(\Delta = 0, \xi_1 = -i, \xi_2 = i) = \begin{pmatrix} \cos\left(\frac{\Omega t}{2}\right) & -\sin\left(\frac{\Omega t}{2}\right) \\ \sin\left(\frac{\Omega t}{2}\right) & \cos\left(\frac{\Omega t}{2}\right) \end{pmatrix}. \tag{4.37}$$

The R_z gate is achieved by introducing detuning, and can be obtained, apart from a global phase shift, by

$$\begin{aligned} R_z = U(\Omega = 0) &= e^{i\Delta t/2} \begin{pmatrix} \cos\left(\frac{\Delta t}{2}\right) - i\sin\left(\frac{\Delta t}{2}\right) & 0 \\ 0 & \cos\left(\frac{\Delta t}{2}\right) + i\sin\left(\frac{\Delta t}{2}\right) \end{pmatrix} \\ &= e^{i\Delta t/2} \begin{pmatrix} e^{-i\Delta t/2} & 0 \\ 0 & e^{i\Delta t/2} \end{pmatrix}. \end{aligned} \tag{4.38}$$

The noise channels in this case are decays from $|0\rangle$ and $|1\rangle$ to states outside the computational basis and we assume that the Rydberg state is always empty for the single-body case. Since both $|r\rangle$ and $|d\rangle$ are not involved in any dynamics, the extension of equation 4.35 to the discussed four level system is straight forward,

$$U = e^{i/2\Delta t} \begin{pmatrix} \cos\left(\Omega'/2t\right) - i\frac{\Delta}{\Omega'}\sin\left(\Omega'/2t\right) & -i\frac{\Omega\xi_1}{\Omega'}\sin\left(\Omega'/2t\right) & 0 & 0 \\ -i\frac{\Omega\xi_2}{\Omega'}\sin\left(\Omega'/2t\right) & \cos\left(\Omega'/2t\right) + i\frac{\Delta}{\Omega'}\sin\left(\Omega'/2t\right) & 0 & 0 \\ 0 & 0 & 1 & 0 \\ 0 & 0 & 0 & 1 \end{pmatrix}. \tag{4.39}$$

The Kraus operators for relaxation of the relevant states are determined by

$$K_i = \sqrt{\gamma_i}\,|d\rangle\langle i|\,. \tag{4.40}$$

Here, we show explicitly how to obtain the Lindblad operator for amplitude damping of the $|0\rangle$ state,

$$L_{0,s} = U^\dagger \epsilon_1 K_0 U, \tag{4.41}$$

which yields

$$L_{0,s} = -\epsilon_a \frac{e^{i\Delta t/2}}{\Omega'} \begin{pmatrix} 0 & 0 & 0 & 0 \\ 0 & 0 & 0 & 0 \\ 0 & 0 & 0 & 0 \\ \left(i\Delta\sin\left(\frac{\Omega' t}{2}\right) - \Omega'\cos\left(\frac{\Omega' t}{2}\right)\right) & i\Omega\xi_1\sin\left(\frac{\Omega' t}{2}\right) & 0 & 0 \end{pmatrix}, \tag{4.42}$$

with $\epsilon_a = \sqrt{\gamma_a}$. The Lindblad operator for pure dephasing is determined similarly, with

$$K_{dp} = \sqrt{\gamma_{dp}} \begin{pmatrix} 1 & 0 & 0 & 0 \\ 0 & -1 & 0 & 0 \\ 0 & 0 & 0 & 0 \\ 0 & 0 & 0 & 0 \end{pmatrix}. \tag{4.43}$$

After having obtained the relevant Lindblad operators in the interaction picture, we can implement everything in the protocol. In figure 4.4, we show the results of the single-qubit implementation. Using a Rabi frequency of $\Omega/2\pi = 10$ kHz and detuning $\Delta = 0$, we find the exact gate time t_g to drive an X-gate by choosing $\Omega t = \pi$ in eq. 4.36, resulting in $t_g = 50$ µs. The result is the gate $U = -i\sigma_x$, similar to the single-qubit gate in the superconducting qubit.
In this case, the amplitude damping channel irreversibly drives the system into the dark-state. We thus end up with both ρ_{00} and ρ_{11} going towards zero as times passes. Dephasing has the most contribution, and we can see the evolution towards the totally mixed state before amplitude damping has had a considerable effect. This is due to the large difference in the two characteristic decay times.

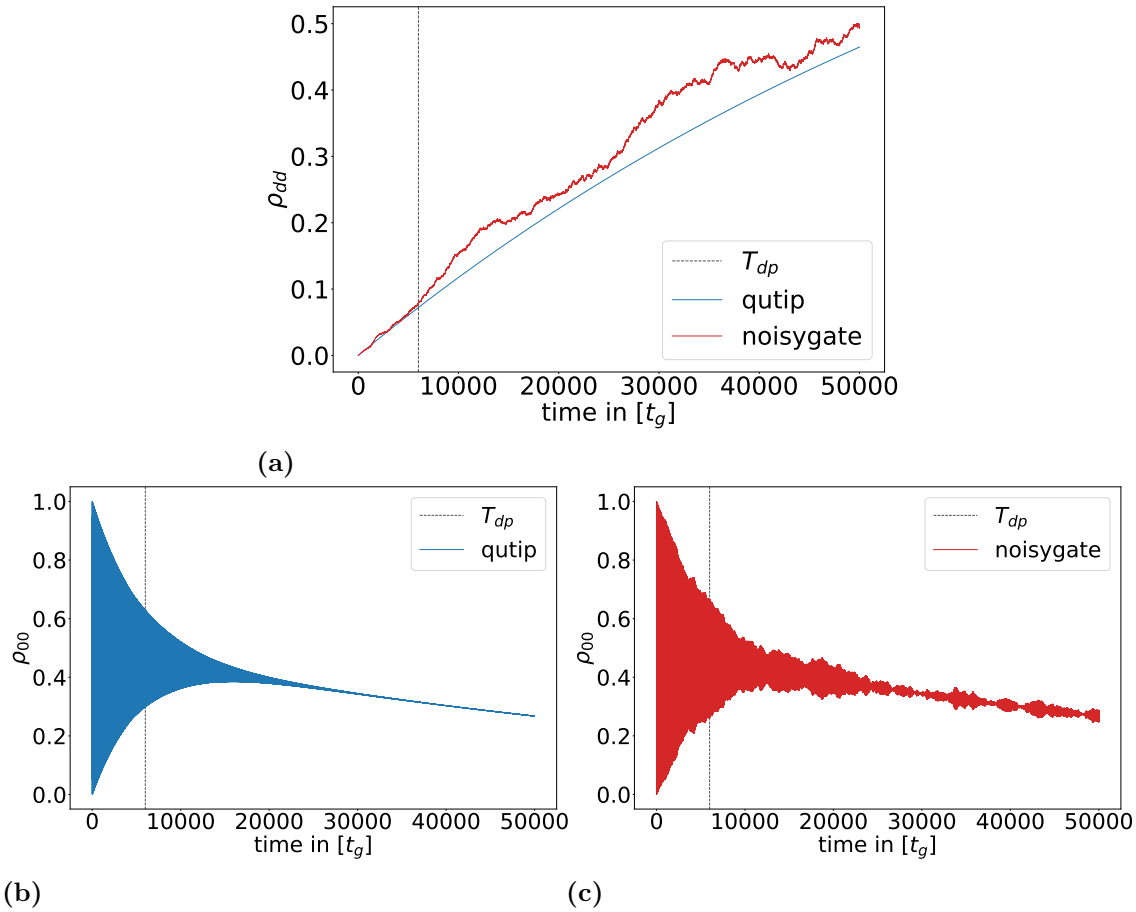

Figure 4.4: In (a), we show how the dark-state continuously gets filled, (b) and (c) show the evolution of the $|0\rangle$ state undergoing Rabi oscillations. For the evolution, we use Rabi frequency $\Omega/2\pi = 10$ kHz, detuning $\Delta = 0$, lifetime of both states $T_a = 4$ s and dephasing time $T_{dp} = 300$ ms.

4.4.2 Two-qubit gate

We show here how to extend the framework of the noisy gates to the case of the two-qubit gates for Rydberg atoms. As the work is still in progress we just show a preliminary results in this direction.
In terms of operators we can write the Hamiltonian

$$H_0 = \hbar\frac{\Omega(t)}{2}(\sigma^+ e^{i\mathbf{kr}} + \sigma^- e^{-i\mathbf{kr}}) - \Delta(t)n, \tag{4.44}$$

with $n = |r\rangle\langle r|$ the projector onto the Rydberg state. If instead we are dealing with N atoms we can extend straight forwardly to

$$H = H_0 + H_{int} \tag{4.45}$$

$$= \hbar \sum_{i=1}^{N} \left[\frac{\Omega(t)}{2} (\sigma_i^+ e^{i\mathbf{k}\mathbf{r}_i} + \sigma_i^- e^{-i\mathbf{k}\mathbf{r}_i}) - \Delta(t) n_i \right] + H_{int}. \tag{4.46}$$

With a newly introduced interaction term H_{int}.
For two atoms, it is simply written as

$$H_{int} = V |n_1\rangle\langle n_2| , \tag{4.47}$$

where we introduce the previously discussed Van-der-Waals interaction term $V = C_{6,r-r}/R^6$ and $|n_1\rangle\langle n_2| = |rr\rangle\langle rr|$.
This results in a two-qubit Hamiltonian, written as

$$\hat{H} = \hat{H}_0 + \hat{H}_{int} \tag{4.48}$$

$$= \hbar \sum_{i=1}^{N} \left[\frac{\Omega(t)}{2} (\sigma_i^+ e^{i\mathbf{k}\mathbf{r}_i} + \sigma_i^- e^{-i\mathbf{k}\mathbf{r}_i}) - \Delta(t) n_i \right] - \frac{C_{6,r-r}}{R^6} |n_1\rangle\langle n_2| , \tag{4.49}$$

where now Ω couples $|1\rangle$ and $|r\rangle$ of both atoms equivalently and thus $|0\rangle$ does not take part in the dynamics. The detailed dynamics look as following [32]. The initial state $|00\rangle$ is uncoupled, thus takes no part in the dynamics. If instead, one of the atoms is initialized in the state $|0\rangle$, the other atom in the $|1\rangle$ state, the second atom undergoes Rabi oscillations with frequency Ω. Lastly, if both atoms are initialized in the excited state, i.e. $|11\rangle$, the Van-der-Waals interaction term modifies the dynamics. In the strong interaction regime $\frac{C_{6,r-r}/R^6}{\Omega} \gg 1$, we effectively achieve a Rabi oscillation between $|11\rangle$ and $|\psi_+\rangle = (|1r\rangle + |r1\rangle)/\sqrt{2}$. In this case, the Rabi frequency is enhanced and we have to be cautious about this when constructing the pulse sequences for driving different gates, which in general are more complex, i.e. both Ω and Δ have time-dependent shapes in general [39]. In this first simulation, we drive the system in the strong interaction regime and, for simplicity, we choose $\mathbf{k}\mathbf{r}_i = 0$ and we choose a constant Rabi frequency and zero detuning. Another important point is, that now we are dealing with $4^2 = 16$ states

in our computational basis, which means in order to obtain the time-evolution operator explicitly, we would have to diagonalize a 16x16 matrix. For these cases, we thus convert to modifying the code and instead, obtain the time-evolution numerically, with all parameters explicitly chosen. In our simulation, we assume that cross-talks are negligible and only consider the amplitude damping channel from the excited Rydberg state of both atoms

$$K_a^{(r,i)} = K_a^r \otimes \mathbb{1}, \tag{4.50}$$

$$K_a^{(i,r)} = \mathbb{1} \otimes K_a^r, \tag{4.51}$$

with

$$K_a^r = \sqrt{\gamma_a} \left|d\right\rangle \left\langle r\right|, \tag{4.52}$$

where γ_a is the rate from the spontaneous decay of the Rydberg state. We note that, for a realistic description, there are more noise channels such as dephasing from various sources that have to be taken into account, as described e.g. in [40]. For now, we only adopt the decay channel from the Rydberg state. We take parameters that resemble realistic conditions, as e.g. in [5]: $T_a = 50\,\mu s$, a gate time of $t_g = 0.5\,\mu s$ and evolve within the strong interaction regime as $V/\Omega = 20$. The resulting dynamics obtained with qutip are displayed in figure 4.5.

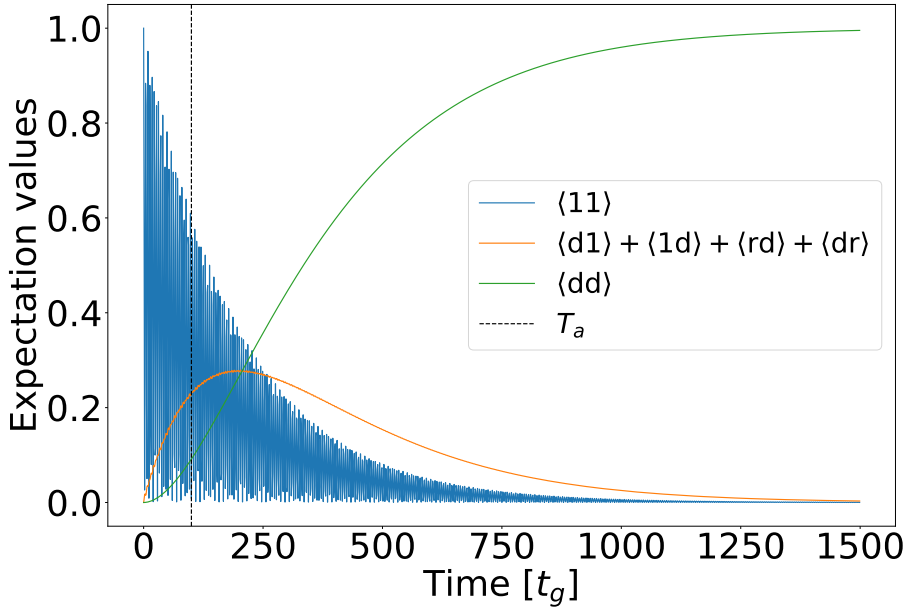

Figure 4.5: We show the expectation value of the $|11\rangle$ state, when driving with the previously defined two-qubit Hamiltonian, using qutip. We have introduced an amplitude damping channel for the Rydberg state with a lifetime of $T_a = 50\,\mu s$ and a gate time of $t_g = 0.5\,\mu s$.

We observe the $|11\rangle$ state and witness the characteristic Rabi oscillations which gradually dampen over time. Concurrently, the $|dd\rangle$ state exhibits a progressively increasing occupation.

5

Conclusion and outlook

In this thesis, we followed the methodology proposed by [6] to incorporate Markovian noise into a gate-like formulation. Our initial focus was on demonstrating the integration of various noise terms, such as relaxation and dephasing, into single-qubit and two-qubit operations by explicitly defining gates. We thoroughly discussed the primary noise contributions within the architecture and showcased the application of the noisy gate protocol using the superconducting qubit as an illustrative example.

Having established the effectiveness of our algorithm in reproducing qualitative behavior consistent with the exact solution to the underlying Lindblad equation for both single-qubit and two-qubit systems, we progressed to apply the formalism to a novel quantum hardware example: the Rydberg atoms. On this hardware, we make use of exaggerated properties of Rydberg atoms for quantum information. The results for the single-qubit showed again good agreement with the predictions. The two-qubit gate will be implemented in the future.

Now that we know we can reproduce the exact dynamics, the next step is to compare the algorithm with physical architectures to see how accurate the simulation performs versus the real implemented gates and see if under the assumptions made in the derivation, we can accurately predict the various contributions to decoherence within the computation. We emphasize that, although we have shown evolutions as far as to the steady state solutions, the regions where $t < T_i$ are most

interesting from a practical point of view. Moving forward, we plan to implement real quantum algorithms, such as the quantum Fourier transform, using the noisy gate formalism.

Moreover, the protocol itself can be extended in many directions. Firstly, we can implement more complicated noise models, sch as including correlated noise in the two-qubit gates or include more general non-Markovian noise, in order to also examine how relevant such noise is in the computers. Another direction is, to implement more complex pulse shapes. With this generalization, we could survey if we can recover the previously reported optimal pulse shapes for driving Rydberg qubits in e.g. [5].

Further insights can also be gained by introducing a function to calculate the entanglement entropy and examining its evolution within our methodology. Lastly, the general applicability of our method allows for exploration across various quantum devices and explore novel directions. Of such could be e.g. the field of photonics [41].

References

[1] J. Preskill, "Quantum computing in the nisq era and beyond," *Quantum*, vol. 2, p. 79, Aug. 2018. [Online]. Available: http://dx.doi.org/10.22331/q-2018-08-06-79

[2] *Quantum Error Correction*. Cambridge University Press, 2013.

[3] Google Quantum AI, "Exponential suppression of bit or phase errors with cyclic error correction," *Nature*, vol. 595, no. 7867, pp. 383–387, Jul. 2021.

[4] M. Morgado and S. Whitlock, "Quantum simulation and computing with rydberg-interacting qubits," *AVS Quantum Science*, vol. 3, no. 2, May 2021. [Online]. Available: http://dx.doi.org/10.1116/5.0036562

[5] A. Pagano, S. Weber, D. Jaschke, T. Pfau, F. Meinert, S. Montangero, and H. P. Büchler, "Error budgeting for a controlled-phase gate with strontium-88 rydberg atoms," *Phys. Rev. Res.*, vol. 4, p. 033019, Jul 2022. [Online]. Available: https://link.aps.org/doi/10.1103/PhysRevResearch.4.033019

[6] G. D. Bartolomeo, M. Vischi, F. Cesa, R. Wixinger, M. Grossi, S. Donadi, and A. Bassi, "A novel approach to noisy gates for simulating quantum computers," 2023.

[7] M. A. Nielsen and I. L. Chuang, *Quantum Computation and Quantum Information: 10th Anniversary Edition*. Cambridge University Press, 2010.

[8] J. Johansson, P. Nation, and F. Nori, "QuTiP 2: A python framework for the dynamics of open quantum systems," *Computer Physics Communications*, vol. 184, no. 4, pp. 1234–1240, apr 2013. [Online]. Available: https://doi.org/10.1016%2Fj.cpc.2012.11.019

[9] F. Campaioli, J. H. Cole, and H. Hapuarachchi, "A Tutorial on Quantum Master Equations: Tips and tricks for quantum optics, quantum computing and beyond," 3 2023.

[10] QuTech. (2023) Rotation operators. [Online]. Available: https://www.quantum-inspire.com/kbase/rotation-operators/

[11] G. Benenti, G. Casati, and G. Strini, *Principles of Quantum Computation and Information: Volume II: Basic Tools and Special Topics*. World Scientific, 03 2007.

[12] C. Gardiner and P. Zoller, *Quantum Noise*. Springer Berlin, 2004.

[13] C. W. Gardiner, *Handbook of stochastic methods for physics, chemistry and the natural sciences*, 3rd ed., ser. Springer Series in Synergetics. Berlin: Springer-Verlag, 2004, vol. 13.

[14] D. J. Griffiths and D. F. Schroeter, *Introduction to Quantum Mechanics, 3rd ed.* Cambridge University Press, 2018.

[15] P. Krantz, M. Kjaergaard, F. Yan, T. P. Orlando, S. Gustavsson, and W. D. Oliver, "A quantum engineer's guide to superconducting qubits," *Applied Physics Reviews*, vol. 6, no. 2, p. 021318, 06 2019. [Online]. Available: https://doi.org/10.1063/1.5089550

[16] *Josephson Junctions*. John Wiley & Sons, Ltd, 2022, ch. 8, pp. 195–210. [Online]. Available: https://onlinelibrary.wiley.com/doi/abs/10.1002/9781119750758.ch8

[17] U. Vool and M. Devoret, "Introduction to quantum electromagnetic circuits," *International Journal of Circuit Theory and Applications*, vol. 45, no. 7, p. 897–934, Jun. 2017. [Online]. Available: http://dx.doi.org/10.1002/cta.2359

[18] G. S. Paraoanu, "Microwave-induced coupling of superconducting qubits," *Phys. Rev. B*, vol. 74, p. 140504, Oct 2006. [Online]. Available: https://link.aps.org/doi/10.1103/PhysRevB.74.140504

[19] S. Sheldon, E. Magesan, J. M. Chow, and J. M. Gambetta, "Procedure for systematically tuning up cross-talk in the cross-resonance gate," *Phys. Rev. A*, vol. 93, p. 060302, Jun 2016. [Online]. Available: https://link.aps.org/doi/10.1103/PhysRevA.93.060302

[20] E. Magesan and J. M. Gambetta, "Effective hamiltonian models of the cross-resonance gate," *Phys. Rev. A*, vol. 101, p. 052308, May 2020. [Online]. Available: https://link.aps.org/doi/10.1103/PhysRevA.101.052308

[21] P. Groszkowski and J. Koch, "Scqubits: a Python package for superconducting qubits," *Quantum*, vol. 5, p. 583, Nov. 2021. [Online]. Available: https://doi.org/10.22331/q-2021-11-17-583

[22] IBM. Compute resrouces. [Online]. Available: https://quantum-computing.ibm.com/services/resources

[23] Qiskit contributors, "Qiskit: An open-source framework for quantum computing," 2023.

[24] X. Wu, X. Liang, Y. Tian, F. Yang, C. Chen, Y.-C. Liu, M. K. Tey, and L. You, "A concise review of rydberg atom based quantum computation and quantum simulation*," *Chinese Physics B*, vol. 30, no. 2, p. 020305, feb 2021. [Online]. Available: https://dx.doi.org/10.1088/1674-1056/abd76f

[25] C. Foot, *Atomic Physics*. Oxford Master Series in Physics, 2005.

[26] T. F. Gallagher, *Rydberg atoms*. Cambridge University Press, 1994.

[27] A. Browaeys and T. Lahaye, "Many-body physics with individually controlled rydberg atoms," *Nature Physics*, vol. 16, pp. 132–142, Jan 2020.

[28] L. Henriet, L. Beguin, A. Signoles, T. Lahaye, A. Browaeys, G.-O. Reymond, and C. Jurczak, "Quantum computing with neutral atoms," *Quantum*, vol. 4, p. 327, sep 2020. [Online]. Available: https://doi.org/10.22331%2Fq-2020-09-21-327

[29] T. L. Nguyen, "Study of dipole-dipole interaction between rydberg atoms : toward quantum simulation with rydberg atoms," PhD thesis, Université Pierre et Marie Curie - Paris VI, 2016, nNT : 2016PA066695, tel-01609840.

[30] M. Saffman, "Quantum computing with atomic qubits and rydberg interactions: progress and challenges," *Journal of Physics B: Atomic, Molecular and Optical Physics*, vol. 49, no. 20, p. 202001, oct 2016. [Online]. Available: https://doi.org/10.1088%2F0953-4075%2F49%2F20%2F202001

[31] D. Jaksch, J. I. Cirac, P. Zoller, S. L. Rolston, R. Côté, and M. D. Lukin, "Fast quantum gates for neutral atoms," *Physical Review Letters*, vol. 85, no. 10, pp. 2208–2211, sep 2000. [Online]. Available: https://doi.org/10.1103%2Fphysrevlett.85.2208

[32] H. Levine, A. Keesling, G. Semeghini, A. Omran, T. T. Wang, S. Ebadi, H. Bernien, M. Greiner, V. Vuletić, H. Pichler, and M. D. Lukin, "Parallel implementation of high-fidelity multiqubit gates with neutral atoms," *Physical Review Letters*, vol. 123, no. 17, Oct. 2019. [Online]. Available: http://dx.doi.org/10.1103/PhysRevLett.123.170503

[33] D. B. Branden, T. Juhasz, T. Mahlokozera, C. Vesa, R. O. Wilson, M. Zheng, A. Kortyna, and D. A. Tate, "Radiative lifetime measurements of rubidium rydberg states," *Journal of Physics B: Atomic, Molecular and Optical Physics*, vol. 43, no. 1, p. 015002, dec 2009. [Online]. Available: https://doi.org/10.1088%2F0953-4075%2F43%2F1%2F015002

[34] J. Yang, X. He, R. Guo, P. Xu, K. Wang, C. Sheng, M. Liu, J. Wang, A. Derevianko, and M. Zhan, "Coherence preservation of a single neutral atom qubit transferred between magic-intensity optical traps," *Phys. Rev. Lett.*, vol. 117, p. 123201, Sep 2016. [Online]. Available: https://link.aps.org/doi/10.1103/PhysRevLett.117.123201

[35] C. Sheng, X. He, P. Xu, R. Guo, K. Wang, Z. Xiong, M. Liu, J. Wang, and M. Zhan, "High-fidelity single-qubit gates on neutral atoms in a two-dimensional magic-intensity optical dipole trap array," *Phys. Rev. Lett.*, vol. 121, p. 240501, Dec 2018. [Online]. Available: https://link.aps.org/doi/10.1103/PhysRevLett.121.240501

[36] J. D. Thompson, T. G. Tiecke, A. S. Zibrov, V. Vuletić, and M. D. Lukin, "Coherence and raman sideband cooling of a single atom in an optical tweezer," *Phys. Rev. Lett.*, vol. 110, p. 133001, Mar 2013. [Online]. Available: https://link.aps.org/doi/10.1103/PhysRevLett.110.133001

[37] K. Wintersperger, F. Dommert, T. Ehmer, A. Hoursanov, J. Klepsch, W. Mauerer, G. Reuber, T. Strohm, M. Yin, and S. Luber, "Neutral atom quantum computing hardware: performance and end-user perspective,"

EPJ Quantum Technology, vol. 10, no. 1, aug 2023. [Online]. Available: https://doi.org/10.1140%2Fepjqt%2Fs40507-023-00190-1

[38] X. Jiang, J. Scott, M. Friesen, and M. Saffman, "Sensitivity of quantum gate fidelity to laser phase and intensity noise," *Physical Review A*, vol. 107, no. 4, apr 2023. [Online]. Available: https://doi.org/10.1103%2Fphysreva.107.042611

[39] X.-Y. Zhu, E. Liang, and S.-L. Su, "Rydberg-atom-based controlled arbitrary-phase gate and its applications," *J. Opt. Soc. Am. B*, vol. 36, no. 7, pp. 1937–1944, Jul 2019. [Online]. Available: https://opg.optica.org/josab/abstract.cfm?URI=josab-36-7-1937

[40] I. Cong, H. Levine, A. Keesling, D. Bluvstein, S.-T. Wang, and M. D. Lukin, "Hardware-efficient, fault-tolerant quantum computation with rydberg atoms," *Phys. Rev. X*, vol. 12, p. 021049, Jun 2022. [Online]. Available: https://link.aps.org/doi/10.1103/PhysRevX.12.021049

[41] S. Slussarenko and G. J. Pryde, "Photonic quantum information processing: A concise review," *Applied Physics Reviews*, vol. 6, no. 4, p. 041303, 10 2019. [Online]. Available: https://doi.org/10.1063/1.5115814

A

Superconducting qubit

A.1 Derivation of the Josephson equations

We follow the derivation done in [16].
The state of a superconductor can be described by a macroscopic wave function

$$\psi(r) = \sqrt{n}e^{i\theta}, \tag{A.1}$$

where n is the number of Cooper pairs and their density is $\rho = 2q_e n$. In a closed system the wave function obeys the Schrödinger equation,

$$i\hbar\frac{\partial\psi}{\partial t} = U\psi. \tag{A.2}$$

If we now, similar to the Josephson junction, place two superconductors in the vicinity of each other we obtain two coupled equations

$$i\hbar\frac{\partial\psi_1}{\partial t} = U_1\psi_1 + \kappa\psi_2 \tag{A.3}$$

$$i\hbar\frac{\partial\psi_2}{\partial t} = U_2\psi_2 + \kappa\psi_1, \tag{A.4}$$

with the coupling constant κ of the interaction between the two superconductors. Now, we apply the voltage $V/2$ to the first and $-V/2$ to the second superconductor. We assume that both superconductors are equal, therefore $U_1 = U_0 - qV/2$ and $U_2 = U_0 + qV/2$, with $q = 2q_e$ the charge of a Cooper pair. We set U_0 for simplicity and get the expression

$$i\hbar\frac{\partial\psi_1}{\partial t} = \frac{qV}{2}\psi_1 + \kappa\psi_2 \tag{A.5}$$

$$i\hbar\frac{\partial\psi_2}{\partial t} = \frac{-qV}{2}\psi_2 + \kappa\psi_1. \tag{A.6}$$

Substituting the correct form of the wave functions, we obtain

$$i\hbar\frac{\partial n_1}{\partial t} - 2\hbar n_1\frac{\partial\theta_1}{\partial t} = -qVn_1 + 2\kappa\sqrt{n_1 n_2}e^{i\phi}, \tag{A.7}$$

$$i\hbar\frac{\partial n_2}{\partial t} - 2\hbar n_2\frac{\partial\theta_2}{\partial t} = qVn_2 + 2\kappa\sqrt{n_1 n_2}e^{-i\phi} \tag{A.8}$$

with $\phi = \theta_2 - \theta_1$. Next, we uncouple the imaginary and real parts,

$$\frac{\partial n_1}{\partial t} = \frac{2\kappa}{\hbar}\sqrt{n_1 n_2}\sin(\phi) \tag{A.9}$$

$$\frac{\partial n_2}{\partial t} = -\frac{2\kappa}{\hbar}\sqrt{n_1 n_2}\sin(\phi) \tag{A.10}$$

$$\frac{\partial\theta_1}{\partial t} = \frac{qV}{2\hbar} - \frac{\kappa}{\hbar}\sqrt{\frac{n_2}{n_1}}\cos(\phi) \tag{A.11}$$

$$\frac{\partial\theta_2}{\partial t} = -\frac{qV}{2\hbar} - \frac{\kappa}{\hbar}\sqrt{\frac{n_1}{n_2}}\cos(\phi). \tag{A.12}$$

Let us consider a volume that encloses superconductor 1 and passes through the insulator, the continuity equation then yields

$$\oint \mathbf{J}_1 \cdot \mathbf{ds} = -\frac{\partial}{\partial t}\int_V (\rho_1)dV \tag{A.13}$$

$$\rightarrow J_1 A = -\frac{\partial}{\partial t}\int_V -2q_e n_1 dV \tag{A.14}$$

$$= 2q_e\frac{\partial n_1}{\partial t}AW \tag{A.15}$$

$$= 2q_e AW\frac{2\kappa}{\hbar}\sqrt{n_1 n_2}\sin(\phi), \tag{A.16}$$

which can be rewritten using $I_i = J_i A$,

$$I_1 = I_c \sin(\phi). \tag{A.17}$$

We assumed here, that the superconductor has rectangular shape with width W perpendicular to the junction which has area A.
The second equation is obtained, considering the phase factor

$$\frac{\partial \phi}{\partial t} = \frac{\partial \theta_2}{\partial t} - \frac{\partial \theta_1}{\partial t}. \tag{A.18}$$

Again, we consider the two superconductors to be equal, we thus have $n_1 = n_2$ and we can write

$$\frac{\partial \phi}{\partial t} = \frac{2q_e V}{\hbar} = \frac{2\pi}{\Phi_0} V, \tag{A.19}$$

where again $\Phi_0 = h/2q_e$ is the flux quantum. We rewrite the expression in terms of the voltage

$$V = \frac{\Phi_0}{2\pi} \frac{\partial \phi}{\partial t}. \tag{A.20}$$

Finally, the two equations, A.17 and A.20, are the Josephson equations.

A.2 Single gate derivation

Single qubit operations can be implemented by the unitary operator

$$U(\theta, \phi) = e^{-i\theta R_{xy}(\phi)/2}, \tag{A.21}$$

with $R_{xy}(\phi) = \cos(\phi)X + \sin(\phi)Y$ and the corresponding Hamiltonian given by

$$H(\theta, \phi) = \frac{\theta \hbar}{2} R_{xy}(\phi). \tag{A.22}$$

And we introduce the relevant Lindblad operators

$$L_1 = \sqrt{\frac{\lambda_1}{\lambda}}\sigma^-,\ L_2 = \sqrt{\frac{\lambda_2}{\lambda}}\sigma^+,\ L_3 = \sqrt{\frac{\lambda_3}{\lambda}}Z, \tag{A.23}$$

where $\epsilon = \sqrt{\lambda} = \sqrt{\lambda_1 + \lambda_2 + \lambda_3} = \sqrt{(2\gamma_d) + (2\gamma_d + \gamma_1) + (\gamma_d + \gamma_z)}$.
With this we can evaluate the Lindblad operators (jump operators), remembering the property of exponentiation of Pauli matrices (proven simply by Taylor expanding the exponential)

$$e^{i\theta X} = \left[\cos(\theta)\mathbb{1} + i\sin(\theta)X\right], \tag{A.24}$$

which holds for all Pauli matrices as well as in our case replacing X for $R_{xy}(\phi)$. (to prove this we can simply use $\cos^2(\phi) + \sin^2(\phi) = 1$ and $XY + YX = 0$ for combinations of Pauli matrices (anticommutation)). Therefore, for eq. A.21, we have

$$U_s^\dagger = \cos(\theta/2)\mathbb{1} + i\sin(\theta/2)\left(\cos(\phi)X + \sin(\phi)Y\right) \tag{A.25}$$

$$U_s = \cos(\theta)\mathbb{1} - i\sin(\theta)\left(\cos(\phi)X + \sin(\phi)Y\right) \tag{A.26}$$

Then we get (remembering $(e^A)^\dagger = e^{A^\dagger}$ and $(\sigma^k)^\dagger = \sigma^k$)

$$U_s^\dagger\sigma^+U_s = \frac{e^{i\phi}}{2}\left[R_{xy}(\phi) + iR(\overline{2s\theta}, \overline{\phi})\right], \tag{A.27}$$

$$U_s^\dagger\sigma^-U_s = \frac{e^{-i\phi}}{2}\left[R_{xy}(\phi) - iR(\overline{2s\theta}, \overline{\phi})\right], \tag{A.28}$$

$$U_s^\dagger ZU_s = R(2s\theta, \overline{\phi}), \tag{A.29}$$

with $R(\theta, \phi) = \cos(\theta/2)Z + \sin(\theta/2)R_{xy}(\phi)$ ($\overline{\alpha} = \alpha + \pi/2$).
For the third term $L_{3,s} = L_{3,s}^\dagger$, thus it vanishes in the final term

$$\Lambda = -\frac{1}{2}\int_0^1 ds\left[\epsilon_1^2\sigma_s^+\sigma_s^- + \epsilon_2^2\sigma_s^-\sigma_s^+\right], \tag{A.30}$$

because e.g. $\sigma_s^+\sigma_s^+ = U_s^\dagger\sigma^+U_sU_s^\dagger\sigma^+U_s = U_s^\dagger\sigma^+\sigma^+U_s = 0$.
The integral can then be evaluated

$$\int_0^1 ds\sigma_s^+\sigma_s^- = \frac{1}{2}\left[\mathbb{1} + \frac{\sin(\theta/2)}{\theta/2}R(\theta,\overline{\phi})\right], \tag{A.31}$$

which then gives for

$$\Lambda = -\frac{\epsilon_1^2+\epsilon_2^2}{4}\mathbb{1} - \frac{\epsilon_1^2-\epsilon_2^2}{4}\frac{\sin(\theta/2)}{\theta/2}R(\theta,\overline{\phi}). \tag{A.32}$$

Exponentiating this term leads to the desired result.
For the stochastic part we need to sample the random variables. This can be effectively done using standard functions, since the mean of all variables is zero and so only the covariant matrix has to be set up. The variances and correlations are easy Ito integrals and can be evaluated straight forwardly.
We start by expanding the sum

$$\Xi(\theta,\phi) = i\epsilon\sum_{k=1}^{N^2-1}\int_0^1 dW_{k,s}L_{k,s} \tag{A.33}$$

$$= i\epsilon_1\int_0^1 dW_{1,s}\frac{e^{-i\phi}}{2}\left[R_{xy}(\phi) - iR(\overline{2s\theta},\overline{\phi})\right] \tag{A.34}$$

$$+ i\epsilon_2\int_0^1 dW_{2,s}\frac{e^{i\phi}}{2}\left[R_{xy}(\phi) + iR(\overline{2s\theta},\overline{\phi})\right] \tag{A.35}$$

$$+ i\epsilon_3\int_0^1 dW_{3,s}R(2s\theta,\overline{\phi}) \tag{A.36}$$

$$= i\epsilon_1\int_0^1 dW_{1,s}\frac{e^{-i\phi}}{2}R_{xy}(\phi) + \epsilon_1\int_0^1 dW_{1,s}\cos(s\theta+\pi/2)Z\frac{e^{-i\phi}}{2} \tag{A.37}$$

$$+ \epsilon_1\int_0^1 dW_{1,s}\sin(s\theta+\pi/2)R_{xy}(\phi+\pi/2)\frac{e^{-i\phi}}{2} \tag{A.38}$$

$$+ i\epsilon_2\int_0^1 dW_{2,s}\frac{e^{i\phi}}{2}R_{xy}(\phi) - \epsilon_2\int_0^1 dW_{2,s}\cos(s\theta+\pi/2)Z\frac{e^{i\phi}}{2} \tag{A.39}$$

$$- \epsilon_2\int_0^1 dW_{2,s}\sin(s\theta+\pi/2)R_{xy}(\phi+\pi/2)\frac{e^{i\phi}}{2} \tag{A.40}$$

$$+ i\epsilon_3\int_0^1 dW_{3,s}\cos(s\theta)Z + i\epsilon_3\int_0^1 dW_{3,s}\sin(s\theta)R_{xy}(\phi+\pi/2), \tag{A.41}$$

where we used $\sin(\phi + \pi/2) = \cos(\phi)$ and $\cos(\phi + \pi/2) = -\sin(\phi)$.
Then, we can rewrite conveniently in terms of the operators Z and R_{xy}

$$\begin{aligned}\Xi(\theta,\phi) = iZ\left[i\epsilon_1\int_0^1 dW_{1,s}\sin(s\theta)\frac{e^{-i\phi}}{2} - i\epsilon_2\int_0^1 dW_{2,s}\sin(s\theta)\frac{e^{i\phi}}{2} + \epsilon_3\int_0^1 dW_{3,s}\cos(s\theta)\right] \\ + iR_{xy}(\phi)\left[\epsilon_1\int_0^1 dW_{1,s}\frac{e^{-i\phi}}{2} + \epsilon_2\int_0^1 dW_{2,s}\frac{e^{i\phi}}{2}\right] \\ + iR_{xy}(\overline{\phi})\Bigg[-i\epsilon_1\int_0^1 dW_{1,s}\cos(s\theta)\frac{e^{-i\phi}}{2} + \\ i\epsilon_2\int_0^1 dW_{2,s}\cos(s\theta)\frac{e^{i\phi}}{2} + \epsilon_3\int_0^1 dW_{3,s}\sin(s\theta)\Bigg].\end{aligned} \tag{A.42}$$

Instead of the different Ito integrals we are dealing with in the expression, we define normally distributed random variables

$$\xi_{k,+} = \int_0^1 dW_{k,s}\cos(s\theta),\ \xi_{k,-} = \int_0^1 dW_{k,s}\sin(s\theta) \tag{A.43}$$

$$\xi_{k,w} = \int_0^1 dW_{k,s}. \tag{A.44}$$

With these, we get the final expression for the stochastic part as

$$\Xi(\theta,\phi) = if_0 Z + if_1 R_{xy}(\phi) + if_2 R_{xy}(\overline{\phi}), \tag{A.45}$$

with

$$f_0 = \epsilon_3\xi_{3,+} - i\frac{e^{i\phi}\epsilon_2\xi_{2,-} - e^{-i\phi}\epsilon_1\xi_{1,-}}{2} \tag{A.46}$$

$$f_1 = \frac{e^{i\phi}\epsilon_2\xi_{2,w} + e^{-i\phi}\epsilon_1\xi_{1,w}}{2} \tag{A.47}$$

$$f_2 = \epsilon_3\xi_{3,-} - i\frac{e^{i\phi}\epsilon_2\xi_{2,+} - e^{-i\phi}\epsilon_1\xi_{1,+}}{2}. \tag{A.48}$$

The variances and correlations are computed straight forwardly using the property of the Wiener measure $dW_k dW_j = dt\delta_{kj}$ (they are statistically independent),

$$\langle \xi_{k,\pm} \xi_{j,\pm} \rangle = \frac{1}{2} \left[1 \pm \frac{\sin(2\theta)}{2\theta} \right] \delta_{kj}; \tag{A.49}$$

$$\langle \xi_{k,+} \xi_{j,-} \rangle = \frac{1 - \cos(2\theta)}{4\theta} \delta_{kj}; \tag{A.50}$$

$$\langle \xi_{k,w} \xi_{j,w} \rangle = \delta_{kj}; \tag{A.51}$$

$$\langle \xi_{k,+} \xi_{j,w} \rangle = \frac{\sin(\theta)}{\theta} \delta_{kj}; \tag{A.52}$$

$$\langle \xi_{k,-} \xi_{j,w} \rangle = \frac{1 - \cos(\theta)}{\theta} \delta_{kj}. \tag{A.53}$$

So we can exponentiate this term as well and then arrive at the noisy gate expression

$$N_g = U_g e^{\Lambda} e^{\Xi}. \tag{A.54}$$